Appendix G

Coupling Of EMI To Cables: Theory And Models

University Of York

G.1 Introduction

A major part of the study of coupling paths between mobile communication systems and electronic equipment is the prediction of the level of EMI incident of equipment ports due to external cables. At mobile radio frequencies external cables are generally greater than a wavelength in length and may be the dominant coupling path of EMI into equipment electronics.

A two year work package was undertaken by the University of York to investigate cable coupled EMI at frequencies from 300 MHz to 2.5 GHz. The objectives of the work package were:

1. Quantification of cable coupling at mobile telecommunication frequencies.
2. Construction of models for cable coupling which are able to account for common mode and environmental effects which are expected to be important.
3. Derivation bounds on the level of EMI in cables loads for a number of representative scenarios.

Two fundamental questions to be answered by this research are:

1. For a given antenna and distributed wire network, what are the physical limits of the electromagnetic interaction? Specifically, what is the minimum length scale which needs to be modelled accurately?
2. Assuming that in the general case the cable is longer than the significant coupling length, what is the best method for representing the propagation of the interference signal along the cable out of the coupling region and ultimately into victim devices?

A dual approach of numerical modelling and experimental measurements was used to address these and other questions and to develop the necessary models. This appendix provides an overview of the theoretical and numerical models; the results of the experimental work can be found in Appendix H and Appendix I.

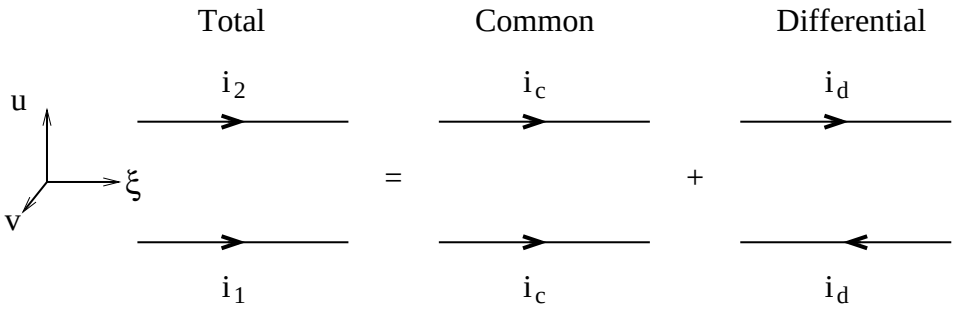

Figure G.1: Definition of differential and common mode currents on a twin wire cable.

G.2 Basic Concepts

An electromagnetic field incident on a cable induces currents on the cable conductors which may interfere with the signal currents leading to timing errors, data errors or even damage to the active components in the cable transceivers. In general the currents on a cable can be decomposed into two components - differential mode and common mode (see Figure G.1) [11]. Consider a two conductor cable with currents $i_1(\xi,t)$ and $i_2(\xi,t)$ flowing on the two wires at distance ξ from one end of the cable. Writing:

$$i_1(\xi,t) = i_c(\xi,t) + i_d(\xi,t) \quad \text{(G.1)}$$

$$i_2(\xi,t) = i_c(\xi,t) - i_d(\xi,t) \quad \text{(G.2)}$$

we can determine the differential mode current, $i_d(\xi,t)$, and common mode current, $i_c(\xi,t)$, to be:

$$i_d(\xi,t) = \frac{1}{2}\left[i_1(\xi,t) - i_2(\xi,t)\right] \quad \text{(G.3)}$$

$$i_c(\xi,t) = \frac{1}{2}\left[i_1(\xi,t) + i_2(\xi,t)\right] \quad \text{(G.4)}$$

Thus at any cross-section of the cable the differential mode currents on the two wires are equal and opposite whereas the common mode currents are equal and in the same direction. The differential mode currents are almost always the functional currents responsible for carrying the signal along the cable. The differential mode currents can be approximated as giving rise to a transverse-electromagnetic wave (TEM) along the cable and hence predicted using standard transmission line theory. However, the common mode currents cannot in general be described by transmission line equations and must be predicted using other techniques. The presence of the common mode currents can be inferred by considering a scattering problem in which an EM field $(\mathbf{E}^i, \mathbf{H}^i)$ is incident on the cable giving rise to a scattered field $(\mathbf{E}^s, \mathbf{H}^s)$. The boundary condition on the surface of the cable conductors requires that the total tangential electric field vanishes:

$$\mathbf{E}^i_{\tan} + \mathbf{E}^s_{\tan} = 0 \quad \text{(G.5)}$$

Since transmission line theory is based on TEM wave propagation, the differential mode currents it predicts can only produce a scattered field with $\mathbf{E}^s_{\tan} = 0$ and thus in general this method

is not able to model the scattering of external fields. The common mode currents are required to provide the component of the scattered field which cancels the incident tangential field on the conductor surfaces.

G.3 Transmission Line Theory

G.3.1 Excited Transmission Line Theory

The voltages and currents on a multi-conductor transmission line, within the approximations of standard transmission line theory, are governed by coupled partial differential equations [1, 5, 11]. For the case of twin wire cables we can write the equations in the frequency domain as:

$$\frac{\partial v^t(\xi,\omega)}{\partial \xi} + zi(\xi,\omega) = v_F(\xi,\omega) \tag{G.6}$$

$$\frac{\partial i(\xi,\omega)}{\partial \xi} + yv^t(\xi,\omega) = i_F(\xi,\omega) \tag{G.7}$$

where the distributed impedance (z) and admittance (y) per unit length are

$$z = r + j\omega l \tag{G.8}$$

$$y = g + j\omega c. \tag{G.9}$$

Here ξ measures the position along the cable, $v^t(\xi,\omega)$ is the total voltage, $i(\xi,\omega)$ is the differential mode current, and l, c, r and g are respectively the inductance, capacitance, resistance and conductance per unit length of the cable. The driving terms are related to the incident electromagnetic field by:

$$v_F(\xi,\omega) = j\omega \int_0^s B_v^i(\mathbf{r},\omega)\, du \tag{G.10}$$

$$i_F(\xi,\omega) = -(g + j\omega c) \int_0^s E_u^i(\mathbf{r},\omega)\, du \tag{G.11}$$

where $\hat{\mathbf{u}}(\xi), \hat{\mathbf{v}}(\xi)$ are unit vectors in the plane perpendicular to the cable at position ξ with $\hat{\mathbf{u}}$ pointing towards the second wire (see Figure G.2). The integrations are in the plane transverse to the cable at position ξ and from one conductor to the other. The excited cable can thus be represented by an equivalent circuit as shown in Figure G.3 with distributed noise sources related to the incident fields [8]. The distributed voltage sources are due to the EMF of the magnetic flux between the two cable conductors and the current sources are due to the displacement current of the electric field driving between the wires.

The complex propagation constant of the line, γ, and characteristic impedance, Z_c, are given by [2]:

$$\gamma = \sqrt{zy} = \alpha + j\omega\beta \tag{G.12}$$

$$Z_c = \sqrt{z/y} \tag{G.13}$$

where $\beta = 2\pi/\lambda$ is the wave number and α is the attenuation constant.

The resistance per unit length, r, is due to the finite conductivity of the cable conductors and is a function of frequency due to the skin effect. The internal inductance of the wires also contributes to the total inductance per unit length. The conductance, g, is due to the dielectric

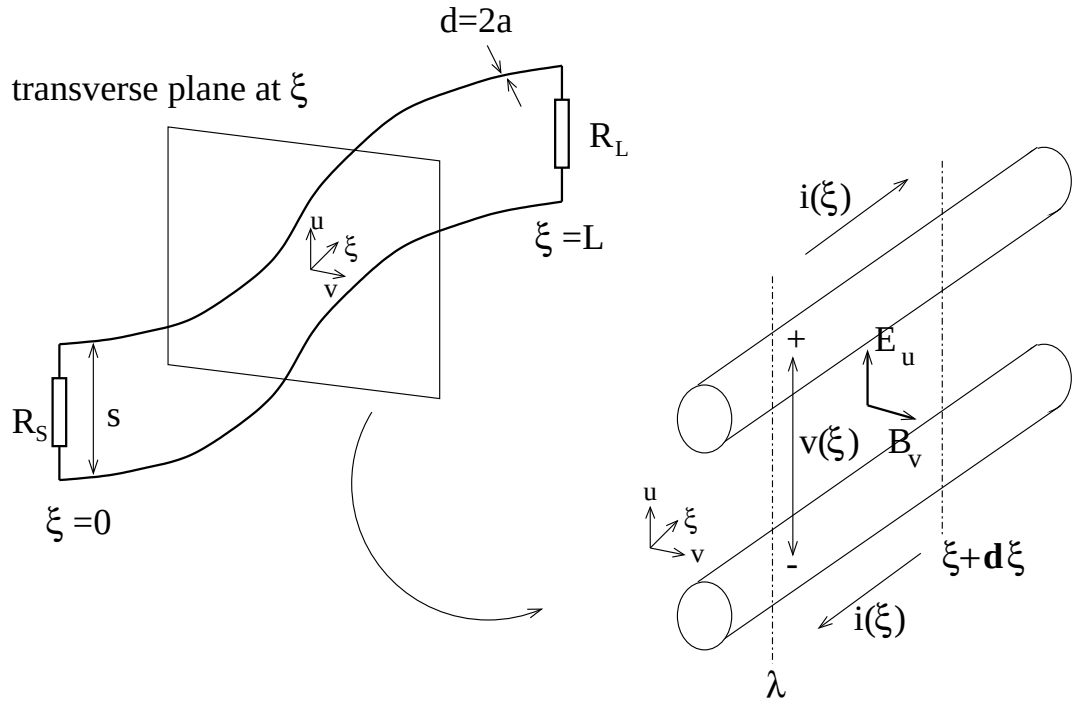

Figure G.2: Excitation of a cable by an external electromagnetic field.

loss of the medium surrounding the cable conductors. Signals on the cable are subject to these losses with an attenuation factor of [2, pp.90]

$$\alpha = \frac{r}{2Z_c} + \frac{gZ_c}{2} \quad (\mathrm{Np\,m^{-1}}) \tag{G.14}$$

The attenuation in decibels per metre is related to that in Nepers per metre by

$$\alpha\,(\mathrm{dB\,m^{-1}}) = 20\log_{10} e \times \alpha\,(\mathrm{Np\,m^{-1}}) \tag{G.15}$$

$$\approx 8.686\,\alpha\,(\mathrm{Np\,m^{-1}}) \tag{G.16}$$

The formalism of this section can easily be extended to multi-wire transmission lines, see for example [8, 5].

G.3.2 Parallel Wire Cable Parameters

Unshielded parallel wire cables provide a worst case for direct differential mode coupling and were therefore used to provide an upper bound on this type of interference. The per unit length parameters of a parallel wire transmission line with conductors of conductivity σ in a medium with permittivity

$$\epsilon = \epsilon' - j\omega\epsilon'' = \epsilon'(1 - j\tan\delta) \tag{G.17}$$

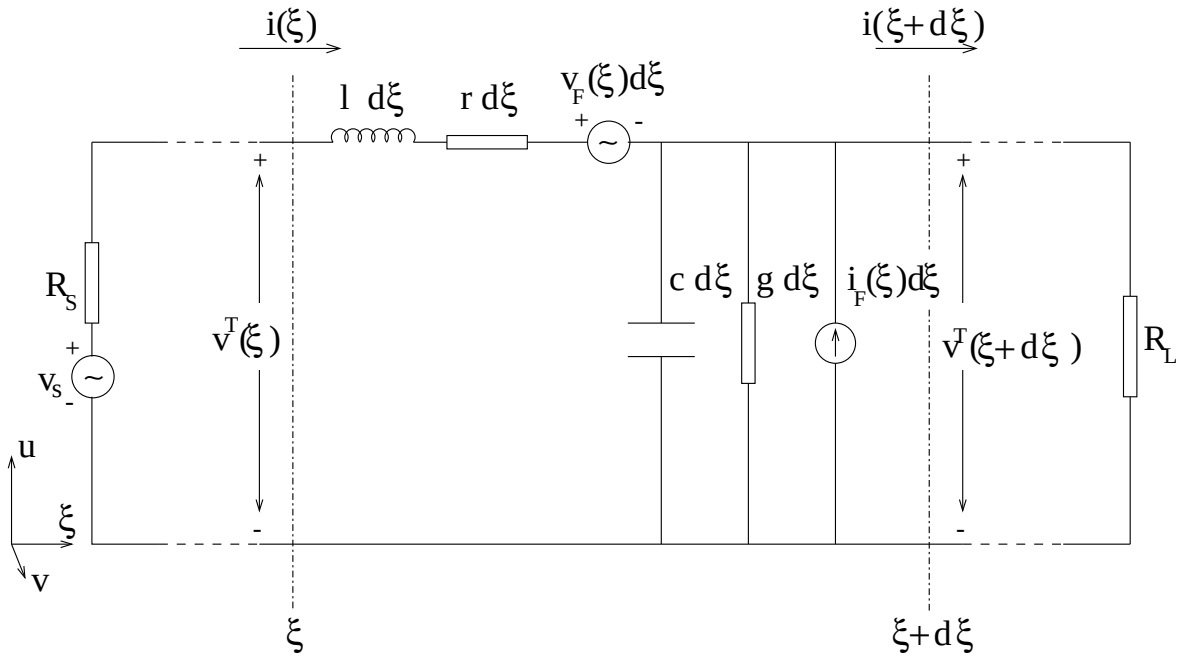

Figure G.3: Equivalent circuit of an excited twin wire cable.

and permeability μ are [2, pp.60]

$$c = \frac{\pi\epsilon}{\cosh^{-1}(s/d)} \tag{G.18}$$

$$l = \frac{\mu}{\pi}\cosh^{-1}(s/d) \tag{G.19}$$

$$r = \frac{2R_s}{\pi d}\left(\frac{s/d}{\sqrt{(s/d)^2-1}}\right) \tag{G.20}$$

$$\approx \frac{2R_s}{\pi d} \tag{G.21}$$

$$g = \frac{\pi\omega\epsilon''}{\cosh^{-1}(s/d)} \tag{G.22}$$

where $\tan\delta = \epsilon''/\epsilon'$ is the loss tangent of the dielectric. Here R_s is the surface impedance of the cable conductors given by

$$R_s = \frac{1}{\sigma\delta_s} = \sqrt{\frac{\omega\mu}{2\sigma}} \tag{G.23}$$

where δ_s is the skin depth

$$\delta_s = \sqrt{\frac{2}{\omega\mu\sigma}}. \tag{G.24}$$

s (mm)	d (mm)	Z_c (Ω)	ϵ_{eff}	α (dBm^{-1})		
				100 MHz	1 GHz	2 GHz
3	2	115	1	0.03	0.1	0.13
6	2	212	1	0.017	0.05	0.08
0.9	0.54	100	1.7	0.13	0.42	0.58

Table G.1: Parallel wire cable parameters. The attenuation is calculated from (G.27) assuming the conductivity is that of copper.

For low loss lines the characteristic impedance, wave number and attenuation constant are:

$$Z_c = \frac{\eta}{\pi}\cosh^{-1}(s/d) \tag{G.25}$$

$$\begin{aligned}\beta &= \omega\sqrt{\mu\epsilon'} \\ &= \frac{\omega}{v_p}\end{aligned} \tag{G.26}$$

$$\alpha = \sqrt{\frac{\omega\mu}{2\sigma}}\frac{1}{\pi d Z_c} + \frac{\pi}{\lambda}\tan\delta \quad (\text{Np m}^{-1}) \tag{G.27}$$

where $v_p = 1/\sqrt{\mu\epsilon'}$ is the phase velocity.

Table G.1 shows the parameters for a number of parallel wire cables investigated during the project. The last entry corresponds to Category 5 (CAT-5) ethernet cable.

The attenuation constants determined by these equations are only accurate at low frequencies. At high frequencies the cable loss is dominant by inhomogeneities in the cable construction giving much higher attenuation than those predicted by this simple model [3]. Measured differential mode attenuation data for CAT-5 UTP cables can be found in Appendix H. The loss at mobile telecommunication frequencies is typically over 10 dB m^{-1}.

G.3.3 Solution For Short Cables

For an electrically short cable, $L << \lambda$, we can use a single section of the equivalent circuit in Figure G.3. Further, providing the termination impedances are not extreme (short or open circuits) we can ignore the per unit length inductance and capacitance of the cable and use the simple equivalent circuit in Figure G.4 to estimate the termination voltages.

For most practical cables the wire separation, s, is much shorter than the cable length L and is therefore also electrically short. The electric and magnetic fields are therefore almost constant across the cable cross section and we can approximate the integrals in equations (G.10) and (G.11) by

$$v_F(\omega)L \approx j\omega\mu_0 H_v^i L s \tag{G.28}$$

$$i_F(\omega)L \approx -j\omega c E_u^i L s. \tag{G.29}$$

From the equivalent circuit the terminal voltages are then [1, pp.429]

$$v_S(\omega) = \frac{R_S}{R_S+R_L}v_F L + \frac{R_s R_L}{R_S+R_L}i_F L \tag{G.30}$$

$$v_L(\omega) = -\frac{R_L}{R_S+R_L}v_F L + \frac{R_s R_L}{R_S+R_L}i_F L. \tag{G.31}$$

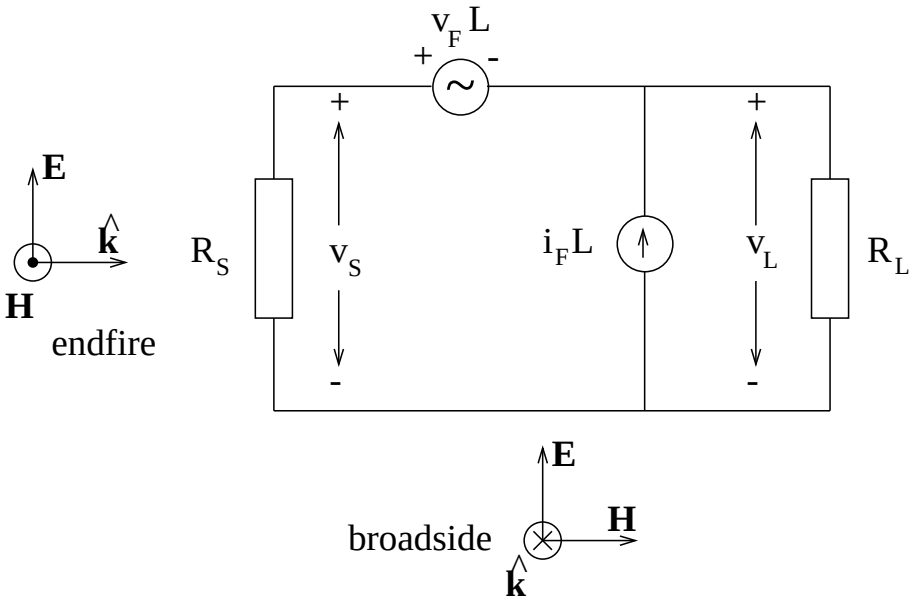

Figure G.4: Equivalent circuit of an electrically short excited twin wire cable of length L.

Consider the special case of end-fire illumination of a matched transmission line by a plane wave of magnitude E. If **E** is polarised in the u direction and hence **H** is in the v direction with magnitude $H = E/\eta$ then it can be shown that

$$|v_S(\omega)| = 0 \tag{G.32}$$

$$|v_L(\omega)| = \frac{2\pi f L}{c} Es \tag{G.33}$$

assuming an air space cable. The voltage in the source load vanishes due to the cancellation of the contributions from the voltage and current sources. This effect is similar to the coupling of forward and backward waves in crosstalk between a pair of transmission lines [1, pp.492]. The load voltage, v_L, increases linearly with frequency as long as the cable remains electrically short. For illumination from the side of the cable (broad-side) the corresponding result is

$$|v_S(\omega)| = \frac{\pi f L}{c} Es \tag{G.34}$$

$$|v_L(\omega)| = \frac{\pi f L}{c} Es. \tag{G.35}$$

In this case v_S and v_L must be equal due to symmetry and are half that of $|v_L|$ for end-fire illumination.

G.3.4 General Solution

The coupled transmission line equations (G.6) and (G.7) can be solved analytically using a chain matrix approach. The result is [4, 12]

$$\begin{aligned} i(\xi,\omega) &= \frac{Z_c\cosh\gamma(L-\xi)+Z_L\sinh\gamma(L-\xi)}{Z_cD} \\ &\times \int_0^{\xi} K(\xi',\omega)\left[Z_c\cosh\gamma\xi'+Z_S\sinh\gamma\xi'\right]\,d\xi' \\ &+ \frac{Z_c\cosh\gamma\xi+Z_S\sinh\gamma\xi}{Z_cD} \\ &\times \int_{\xi}^{L} K(\xi',\omega)\left[Z_c\cosh\gamma(L-\xi')+Z_L\sinh\gamma(L-\xi')\right]\,d\xi' \\ &+ \frac{1}{D}\left[Z_c\cosh\gamma(L-\xi)+Z_L\sinh\gamma(L-\xi)\right]\int_0^{s} E_u^i(u,0,0,\omega)\,du \\ &+ \frac{1}{D}\left[Z_c\cosh\gamma\xi+Z_S\sinh\gamma\xi\right]\int_0^{s} E_u^i(u,0,L,\omega)\,du \end{aligned} \tag{G.36}$$

where

$$K(\xi,\omega) = E_\xi^i(s,0,\xi,\omega)-E_\xi^i(0,0,\xi,\omega) \tag{G.37}$$

$$D = (Z_cZ_S+Z_cZ_L)\cosh\gamma L+(Z_c^2+Z_SZ_L)\sinh\gamma L. \tag{G.38}$$

The currents in the termination impedances can be determined by setting $\xi=0$ and $\xi=L$ in (G.36) to give:

$$\begin{aligned} i_S(\omega) &= i(0,\omega) \\ &= \frac{1}{D}\int_0^{s} K(\xi,\omega)\left[Z_c\cosh\gamma(L-\xi)+Z_L\sinh\gamma(L-\xi)\right]\,d\xi \\ &+ \frac{1}{D}\left[Z_c\cosh\gamma L+Z_L\sinh\gamma L\right]\int_0^{s} E_u^i(u,0,0,\omega)\,du \\ &- \frac{Z_c}{D}\int_0^{s} E_u^i(u,0,L,\omega)\,du \end{aligned} \tag{G.39}$$

$$\begin{aligned} i_L(\omega) &= i(L,\omega) \\ &= \frac{1}{D}\int_0^{s} K(\xi,\omega)\left[Z_c\cosh\gamma L+Z_S\sinh\gamma L\right]\,d\xi \\ &- \frac{1}{D}\left[Z_c\cosh\gamma L+Z_S\sinh\gamma L\right]\int_0^{s} E_u^i(u,0,L,\omega)\,du \\ &+ \frac{Z_c}{D}\int_0^{s} E_u^i(u,0,0,\omega)\,du \end{aligned} \tag{G.40}$$

and the corresponding terminal voltages are then

$$v_S = i_SZ_S \tag{G.41}$$

$$v_L = i_LZ_L. \tag{G.42}$$

The load voltages can be represented by transfer functions

$$T_{S,L} = \frac{v_{S,L}}{sE_{\text{char}}} \tag{G.43}$$

$$T_{S,L}\,(\text{dB}) = 20\log_{10}\left|\frac{v_{S,L}}{sE_{\text{char}}}\right| \tag{G.44}$$

where E_{char} is a characteristic field strength of the incident electromagnetic field. For example, for a plane wave we can take E_{char} equal to the amplitude of the electric field. For inhomogeneous electromagnetic fields such as that close to a dipole there is no simple choice for E_{char}. The maximum field strength incident on the cable is typically used.

This solution was coded as a MATLAB program with a general plane wave incident field allowing for easy calculation of the transfer function. Figure G.5 shows the transfer function for a matched 5 m 115 Ω parallel wire cable ($s = 1.5$ mm, $d = 2$ mm) illuminated by a plane wave from the $\xi = 0$ (R_S) end (end-fire illumination). The electric field is polarised in the u direction and the magnetic field in the v direction. At low frequencies, where the cable is electrically short the approxmation discussed in Section G.3.3 is valid and gives the low frequency asymptote shown in the figure. For this geometry and with match loads there is no voltage in the source load due to cancellation of the contributions from v_F and i_F.

For broad-side illumination (Figure G.6) with the electric field along ξ and magnetic field along v the source and load voltages are the same due to symmetry. Note that for the end-fire illumination the first maximum in the transfer function corresponds to $L = \lambda/4$ whereas for broadside illumination the first maximum is at $L = \lambda/2$. The frequencies of maximum and minimum transfer are given by

$$f_{\max} = \left(n + \frac{1}{2}\right)\frac{c}{2L} \tag{G.45}$$

$$f_{\min} = n\frac{c}{2L} \tag{G.46}$$

for end-fire illumination and

$$f_{\max} = (2n+1)\frac{c}{2L} \tag{G.47}$$

$$f_{\min} = 2n\frac{c}{2L} \tag{G.48}$$

for broad-side illumination where $n = 0, 1, 2, \ldots$.

G.4 Common Mode Effects

G.4.1 Image Theory

To understand how common mode currents can be generated on a cable consider Figure G.7 which shows a twin wire cable over an ideal ground plane excited by an incident field. We can replace this system using image theory with a four conductor system, the incident field and its image as shown. Providing the spacing between the wires in the original cable, s, is small compared to the height of the cable above ground, h, and the line is much longer than h we can replace each pair of conductors in the image system with a single conductor of radius s and we again have a two conductor line which is open circuited at each end and excited by the original field and its image. We can solve this problem using transmission line theory to give the differential mode current on the image conductors which are then interpreted as the common mode currents on the original cable conductors (assuming the current is distributed equally among the conductors of the original cable).

Note that the effective noise sources driving the common mode current are integrals of the combined incident fields over a distance $2h >> s$ and hence the common mode currents induced on the cable are much greater than the differential mode currents. The superposition of

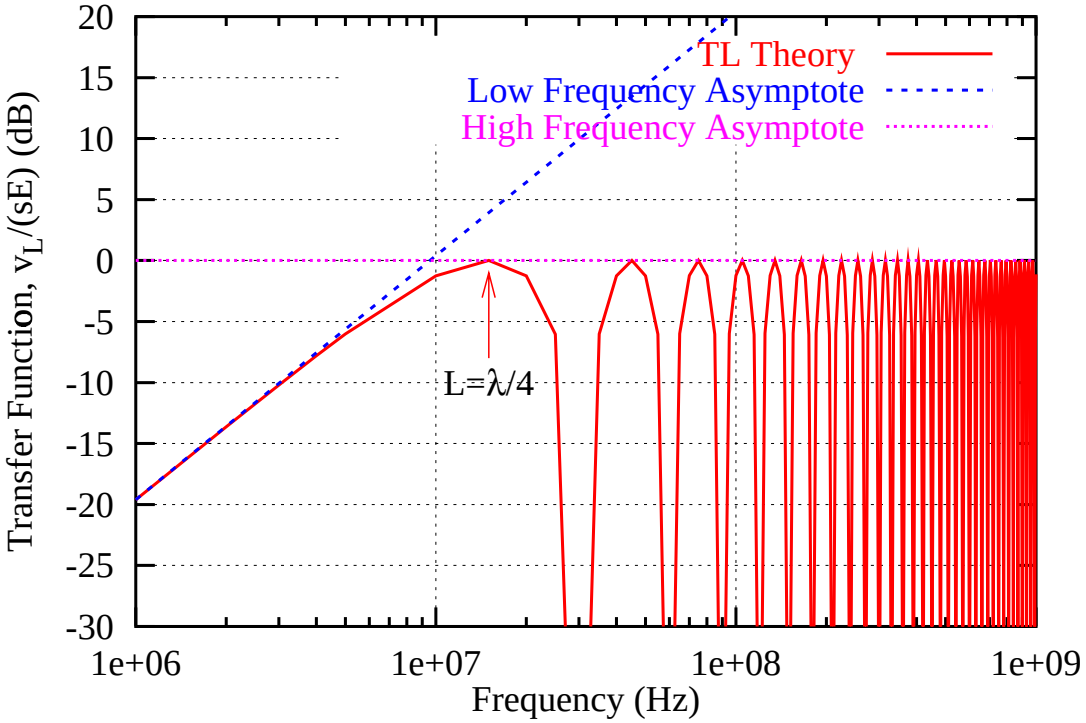

Figure G.5: .Transfer function for a match 5 m 115 Ω parallel wire line with end-fire plane wave illumination. The voltage in the source load is zero in this case due to cancellation of the contributions from v_F and i_F.

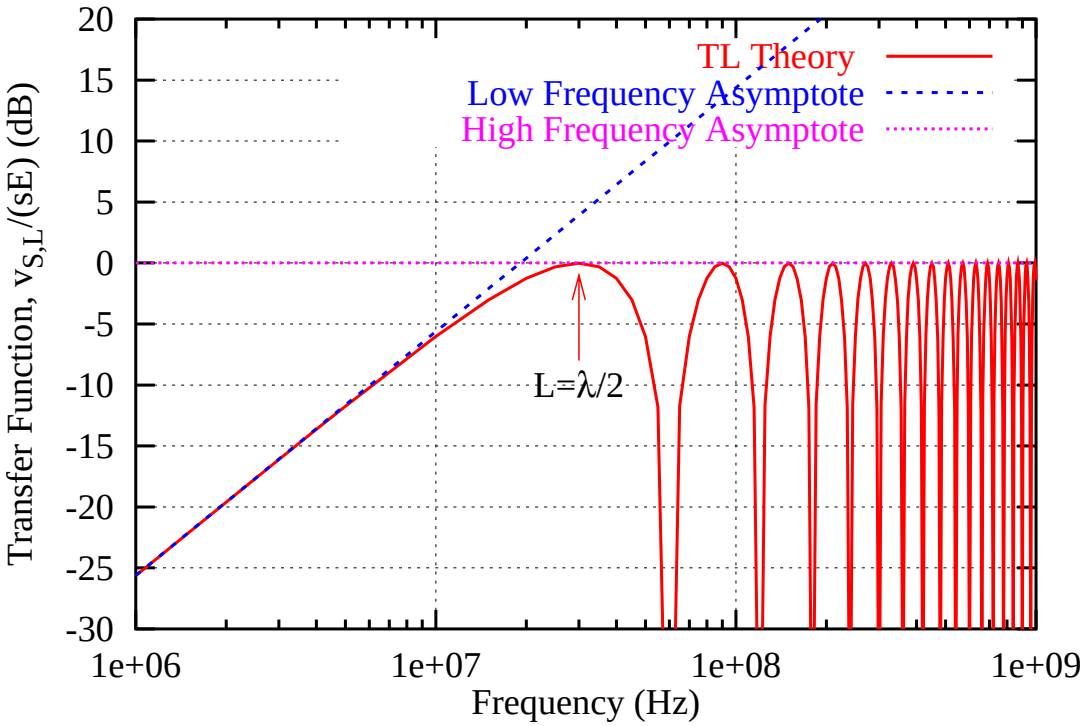

Figure G.6: Transfer functions for a match 5 m 115 Ω parallel wire line with broad-side plane wave illumination.

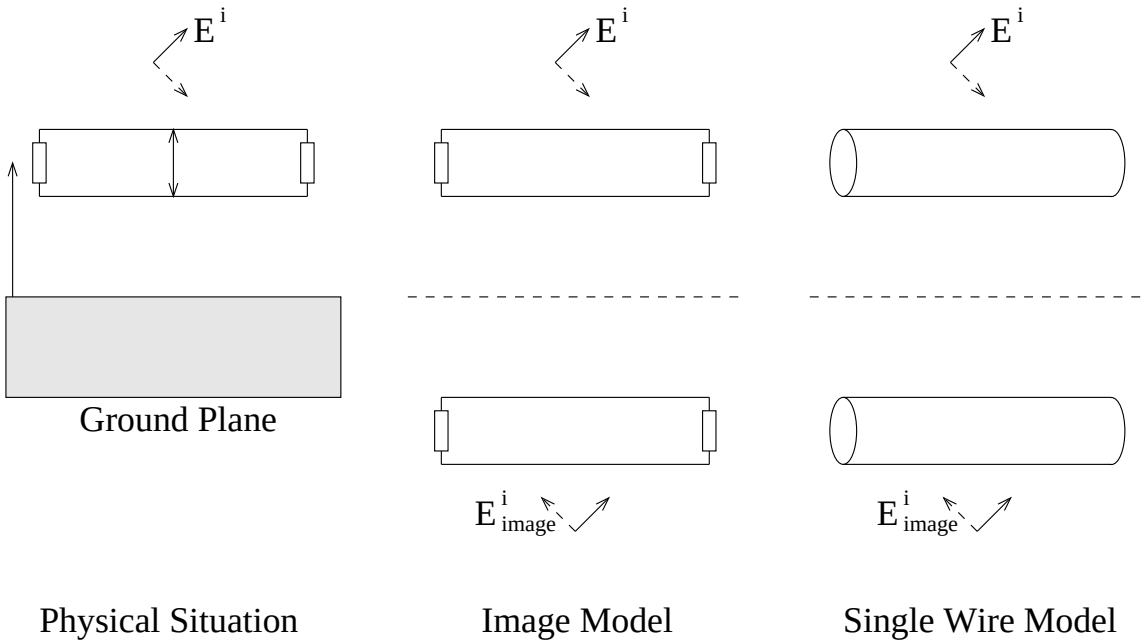

Figure G.7: Image theory model of common mode currents.

the incident field and its image (i.e. ground reflections) will also create an interference pattern in the common mode currents.

The attenuation of the common mode currents as they propagate along the cable is governed by the parameters of image problem and is in general much lower than that of the differential mode currents. However common mode currents are more efficiently re-radiated by the cable which results in higher attenuation than that predicted by the conductor loss alone. The proximity of the ground plane and presence of other metallic object provides guidance for the common mode currents reducing the radiation loss.

Propagation of common mode currents on a cable is thus strongly dependent on the environment in which the cable is placed. Inhomogeneities, re-radiation and reflections all have a large impact on the propagation of the common mode currents. To predict the common mode currents on a real cable therefore requires a more detailed, full-wave, scattering analysis.

G.4.2 Mode Conversion

The presence of common mode currents on a cable does not in itself pose a threat to the integrity of the differential mode data signals. However if any mechanisms exist via which energy can be coupled from common mode into differential mode then the larger magnitudes of the common mode currents can result in this becoming the dominant EMI coupling path. The fundamental mechanism which gives rise to mode conversion is electrical or physical imbalance between the signal carrying conductors in a cable. Consider Figure G.8 which shows how imbalance in the termination of a twin wire line leads to mode conversion.

The common mode currents i_c are incident on a cable termination with resistance R_L. If there are completely balanced return paths for the common mode currents (including capacitive and inductive effects) then there is no differential mode current through the load. However, if the impedance of the common mode return paths is different ($Z_1 \neq Z_2$) then a differential mode current can be generated through the load. The degree of imbalance between the return paths of the two wires determines the amount of common mode current which appears in the cable

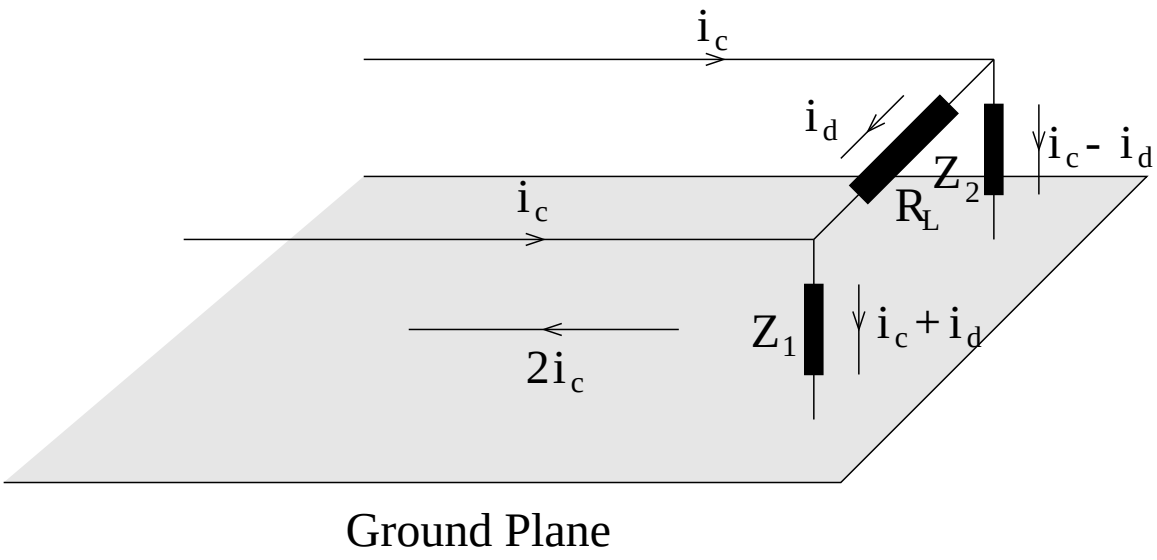

Figure G.8: Schematic mode conversion mechanism at a cable termination.

load. Thus any asymmetry between the two conductors on a two wire cable can lead to common mode currents affecting the data signals.

Note that the imbalance can be caused by different capacitive and inductive couplings between the cable conductors and other conducting objects in the vicinity of the cable. The ground plane itself can cause imbalance on a parallel wire line if the conductors are one above the other relative to the ground.

G.5 Frequency Domain Models

G.5.1 Method Of Moments

We are interested in modelling wired networks which are typically many wavelengths in size. The frequency domain integral equation method applied to thin wires provides an efficient solution for such structures. In view of our existing experience with the method of moments code NEC (Numerical Electromagnetic Code) this package was chosen as the initial modelling tool [13].

In the moment method approach each wire in the system is divided into a number of short segments, each of which is typically chosen to be one tenth of a wavelength long. The total number of such segments in the model, N_{seg}, determines the CPU and memory requirements for the computation.

Initially models were constructed for a simple parallel wire transmission line (PWTL) interacting with a half-wave dipole at 1GHz. This allowed validation of the results (at least for differential mode coupling) against the transmission line theory presented in Section G.3.4.

Although superficially very simple the parallel wire transmission line shown in Figure G.9 presents a number of important problems from a numerical modelling perspective. In the absence of any other external fields or structures the segment length along the wire may be made quite large; past experience suggests that a maximum length of ten times the wire separation may be used before the accuracy begins to deteriorate. However, it is the modelling of the end

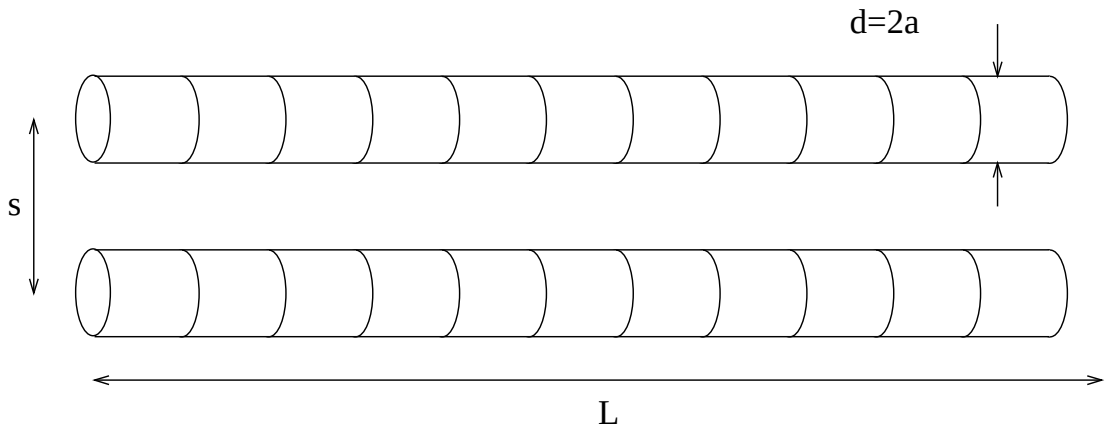

Figure G.9: Parallel wire transmission line model.

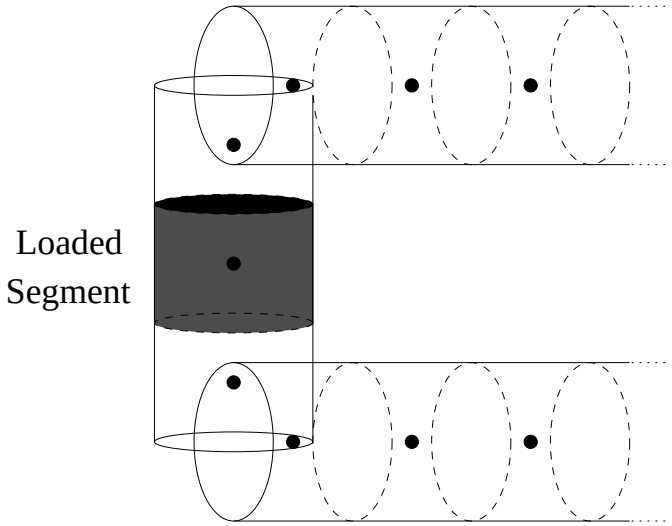

Figure G.10: Detail of segmentation at the line end.

terminations which is critical for attaining reasonable accuracy in the model.

To model the terminating impedances two short wires, with diameters equal to those of the wires along the line, are connected across the line ends. These end wires must in general be divided into an odd number of segments 1, 3,... so that the central segments can be loaded with the required terminating impedances as shown in Figure G.10. It is found that having just one segment on the end wires, so that the loaded segment is in contact with the wires on the line at both of its ends, produces poor results. This indicates that at least three segments are required on the end wires. We also expect to have numerical problems if the segments at the ends of the short connecting wires lie completely 'inside' the wires on the transmission line, i.e. if the segment length is less than the wire radius. For three segments on the end wires this means that we must have $s/a > 3$ and therefore the minimum characteristic impedance which can be modelled by this method is about $115\,\Omega$.

A final consideration is the known problems which occurs with NEC if neighbouring segments have greatly differing lengths. The segment length of the transmission line wires at the

ends of the line must therefore be commensurate with the segment length used on the terminating wires, i.e. about $s/3$. This indicates that dynamic segmentation will be needed to allow larger segment lengths to be used along the majority of the line where it would be very inefficient to use the same segmentation as the end wires.

MATLAB programmes were written to provide a high level interface to NEC for generating dynamically segmented wire structures.

G.5.2 Parallel Wire Models

Two parallel wire lines where chosen for the initial study with characteristic impedances of 115 ΩW and 212 Ω (see Table G.1). Recalling the discussion of the previous section the 115 Ω case is the minimum impedance line which we expect to be able to model accurately using this method.

To assess the accuracy and stability of the modelling procedure the response of a matched $1\frac{1}{4}$ wavelength 212 Ω cable to a 1 V excitation at one end, with matched loads at both ends, was investigated at 1 GHz. Figure G.11 shows the real and imaginary parts of the current obtained on the line for various segmentations compared with the known results from standard transmission line theory. Note that 40 uniform segments along each wire is not enough to give good accuracy in the real part of the current. This is due to the large difference in the segment lengths on the end wires and the neighbouring segments on the line wires. With dynamic segmentation many fewer segments are needed to obtain good accuracy. The slight translation of the numerical predictions for the imaginary part of the current relative to the theoretical curve is due end effects at the terminations.

By looking at the magnitude of the current, which in theory should be constant, we determined the VSWR of the line due to residual (numerical) reflections from the terminations. We found that the VSWR was 1.06 which corresponds to a reflection coefficient of 3%. This can be regarded as a measure of the adequacy of the modelling of the end terminations. The results for the 115 Ω line were very similar with a slightly poorer VSWR of 1.13 (6% reflection).

The pickup of interference on a twenty wavelength 212 Ω line excited by a nearby half-wave dipole was investigated at a frequency of 1 GHz with various orientations of the dipole relative to the line (see Figure G.12). For each orientation the dipole was positioned at a range of both one and three wavelengths from the transmission line and the current induced on the line (with a 1 V source on the dipole) was calculated.

From the EMC point of view it is important to distinguish whether the induced current is in the differential-mode or common-mode. The results obtained for the 212 Ω line at a range of one wavelength show that for this geometry the pickup is generally in the common-mode, though in two cases the differential mode pickup is dominant. The results obtained are summarised in Table G.2.

The differential mode current in configurations 5 and 8 can be predicted using the known solution of the excited transmission line equations G.36. Figure G.13 shows a comparison of the magnitude of the current for configuration 8 obtained from NEC with the theoretical solution using the far field approximation for the dipole fields. The good agreement gives us confidence in our modelling procedure. The region of significant coupling is also clearly identified.

Now consider the common-mode currents. Referring to Table G.2 we see that in the configurations in which they are excited the common-mode currents are an order of magnitude greater than the differential mode currents in configurations 5 and 8; hence we can say that the pickup on a parallel wire transmission line in free space from a nearby dipole is generically in the common-mode. Note that in this model with simple terminating impedances the common-

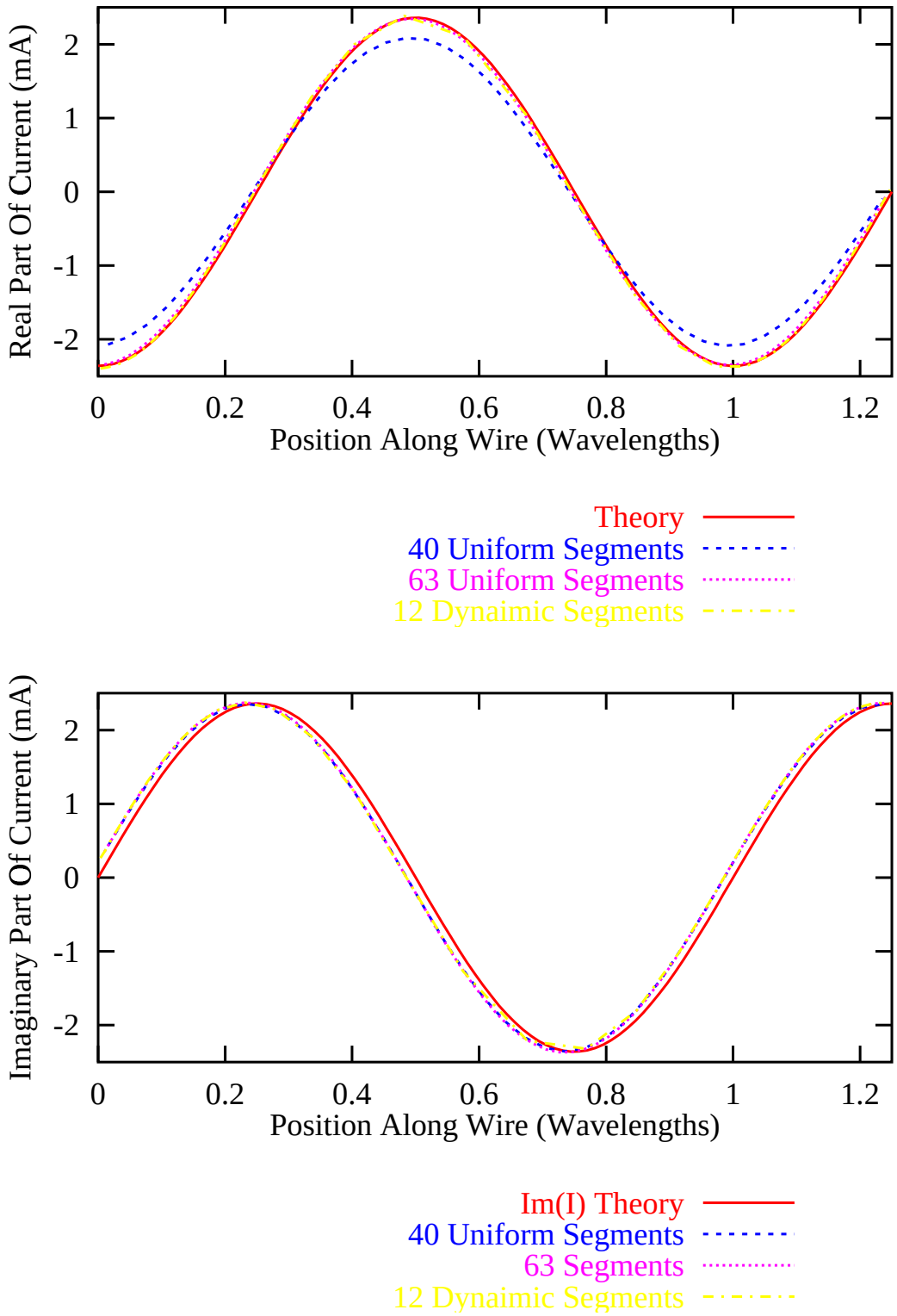

Figure G.11: Response of a one and a quarter wavelength 212 Ω parallel transmission line model to a 1 V excitation at the left hand end. The real and imaginary parts of the current along the cable are shown for uniform and dynamic segmentations compared to ideal transmission line theory.

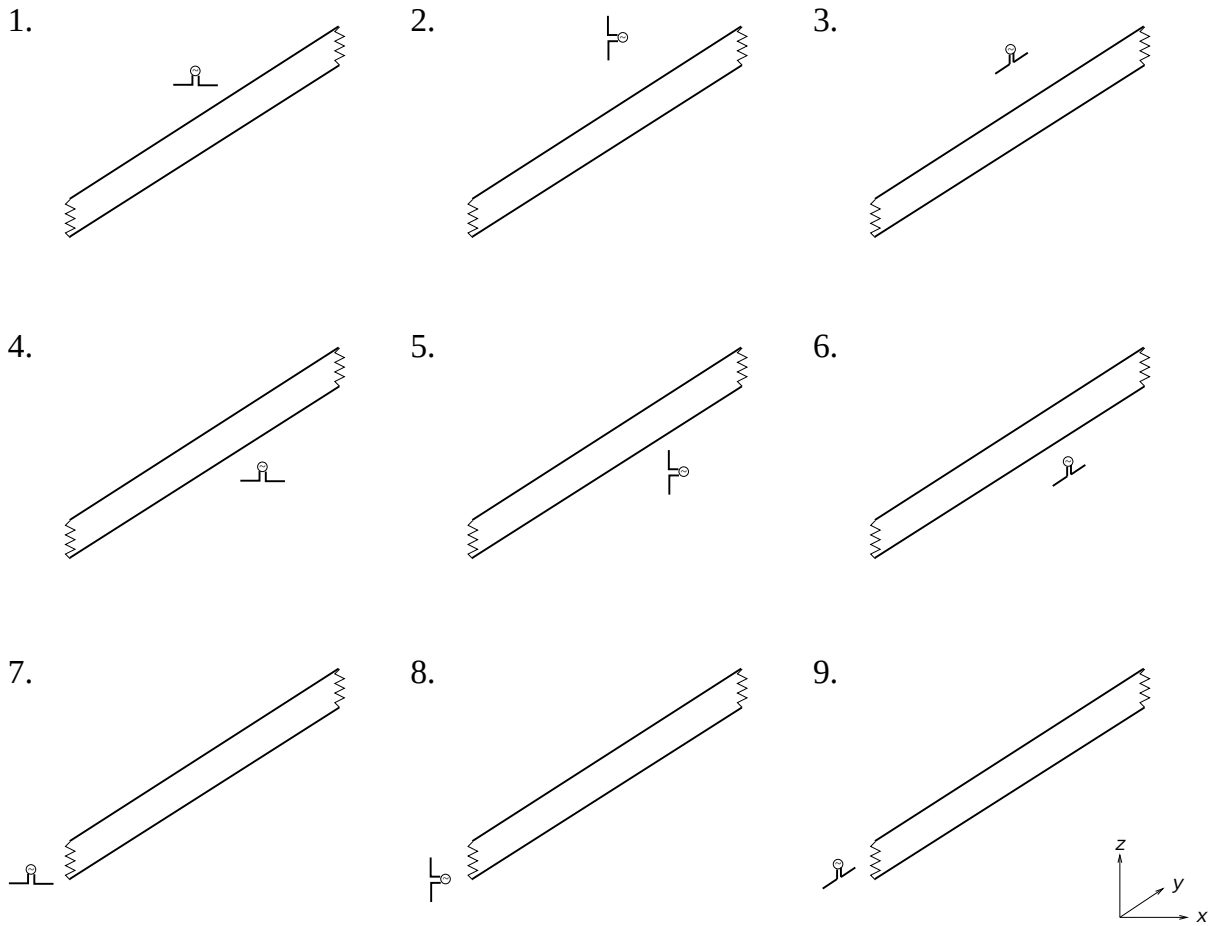

Figure G.12: The nine geometrical orientations of the dipole relative to the transmission line investigated.

mode component of the current cannot appear in the loads as there is no imbalance between the cable wires (the small load currents in configuration 3 are due to a small differential-mode current).

The greatly differing magnitudes and forms of the current in each case highlights the importance of the geometrical orientation of the antenna relative to the transmission line.

Figure G.14 shows the transfer function calculated from NEC for a 5 m 115 Ω cable 1 m above an ideal ground plane illuminated by the inhomogeneous field from a 1 GHz dipole compared to plane wave illumination. The plane wave transfer function is normalised to amplitude of the plane wave, $E_{char} = 1\,\mathrm{Vm}^{-1}$. The dipole transfer function is shown normalised to both $E_{char} = E_{dipole}(f)$ and $E_{char} = E_{dipole}(1\,GHz)$ where $E_{dipole}(f)$ is the electric field strength of the dipole at 1 m. The result with $E_{char} = E_{dipole}(1\,GHz)$ includes the antenna factor of the 1 GHz dipole whereas it is normalised out in the $E_{char} = E_{dipole}(f)$ transfer function. The result demonstrates that assuming a plane wave threat field can significantly over-estimate the threat coupled to cables by sources close to the cable.

To summarise, the method of moments code NEC has been demonstrated to be a suitable tool for the analysis of an antenna interacting with a transmission line at frequencies up to 1 GHz. The initial results show that both differential and common mode currents are excited on a parallel wire transmission line by a half-wave dipole placed at a range of one wavelength. Common mode pickup appears to be the more generic case, however the relative orientation of the dipole and transmission line is important for determining the mode, magnitude and form of

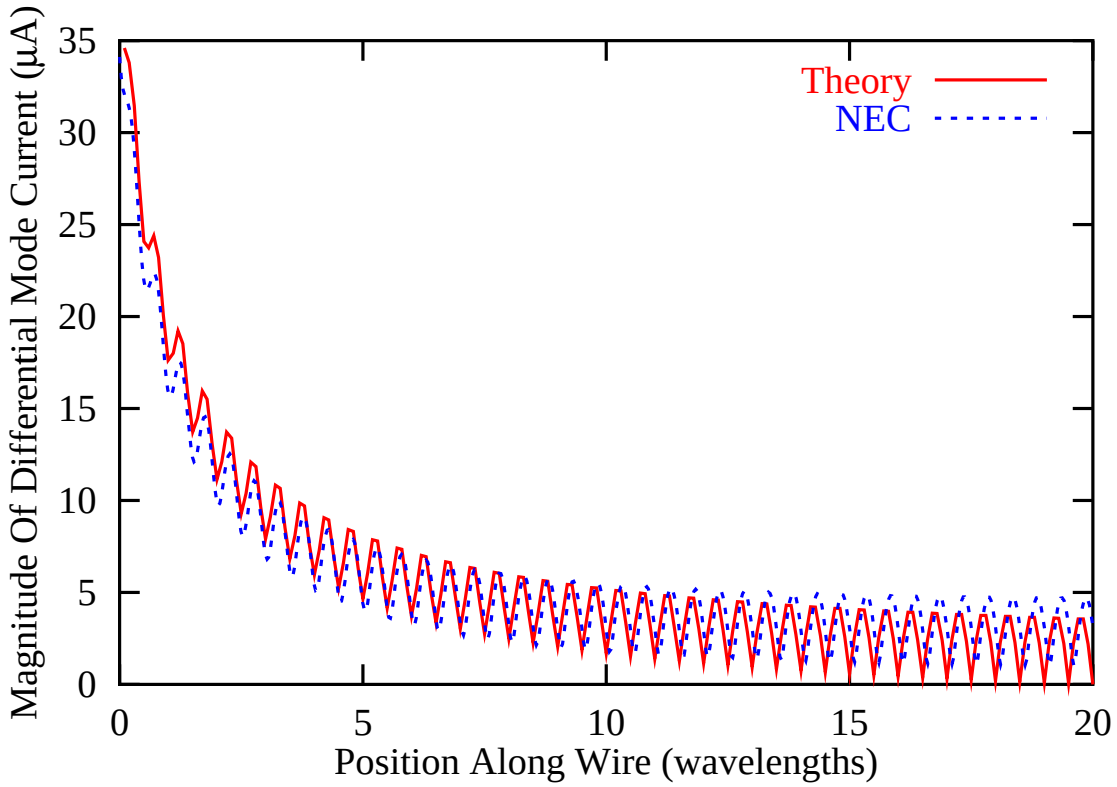

Figure G.13: Comparison of the differential mode current predicted by NEC and theory for configuration 8.

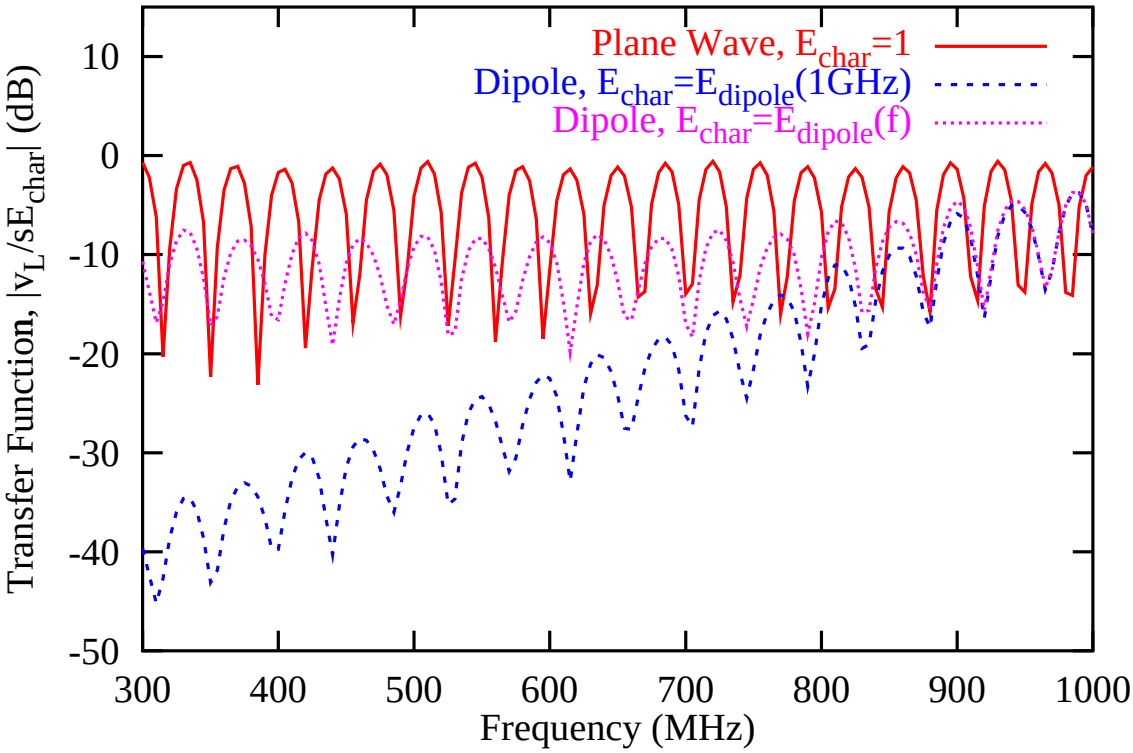

Figure G.14: Comparison of the transfer function of a 5 m cable under oblique incidence from both a plane wave and a 1 GHz half wave dipole.

Configuration	Dominant Mode	Left Load Current (μA)	Right Load Current (μA)	Maximum Current (μA)	Coupling Length (λ)
1	None	-	-	-	-
2	Common	15.2	15.2	500	4
3	Common	0.07	0.07	200	2
4	Common	0	0	500	4
5	Differentail	10.8	10.8	18	2
6	Common	0	0	300	4
7	None	-	-	-	-
8	Differential	34.7	2.8	30	3
9	Common	0	0	250	3

Table G.2: Summary of the results obtained for the current in a 20 wavelength 212 Ω line excited by a dipole source at a range of one wavelength in the nine configurations considered.

the induced current.

G.5.3 Termination Models

In the models so far the PWTL has been simply loaded with matched resistive termination to prevent reflections which might obscure our insight into the pickup on the cable. We now look at how the common-mode current propagates along the line and particularly how it is affected by the presence of metal enclosures and ground planes.

In practice a PWTL carrying a signal into an enclosed device is usually attached to the box by some kind of connector. We will assume for now that the connector is such that one of the wires of the parallel pair sees a low impedance path onto the outer surface of the box whilst the other wire only sees the box through the load resistor. Under these conditions the box may be modelled in NEC by the geometry shown in Figure G.15. The short matching section is to allow the use a course segmentation of the metal box without introducing a rapid variation in segment lengths which can cause numerical problems. This model provides a worst case connector imbalance which can be used, together with the balanced termination, to bound the EMI in the cable loads for a given threat environment.

G.5.4 Models With Mode Conversion

Four different configurations were initially investigated with the unbalanced termination model. (see Figure G.16). In each case a 6 m (20 wavelengths at 1 GHz) 212 Ω PWTL was used with matched resistive terminations. Specifically the four cases are:

A. Metal box on one end of the line

B. Metal box on both ends of the line

C. Line above a perfectly conducting ground plane

D. Metal box on both ends above perfectly conducting ground plane

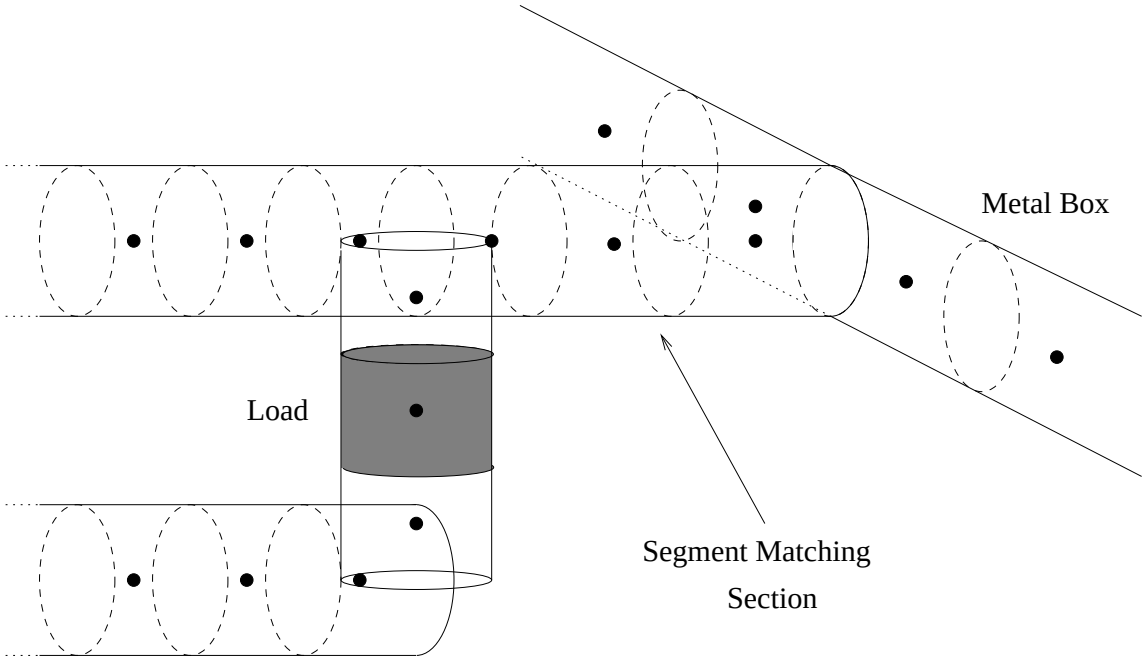

Figure G.15: Geometry of the transmission line/box interface.

The metal boxes were modelled using a cubic wire frame in NEC with side lengths of 0.3 m, 0.45 m and 0.6 m. A more realistic solid box was also considered using a second moment method code (CONCEPT). The antenna orientation and range was varied in the same way as for the free space model.

In each case the important quantities are the differential and common mode currents incident on the resistive loads. As can be seen, with all the variables involved, the parameter space is very large and a subset of cases has to be considered. The following sections summarise the results obtained in each case.

G.5.5 Case A - Box on one end of the line

The presence of the metal box provides an alternative current path for the common-mode current away from the load, thus allowing common-mode to differential-mode conversion to occur at the interface between the transmission line and box . This is of crucial importance from an EMC perspective since it allows the electromagnetic energy to enter the load. In a more realistic model this will correspond to an electromagnetic interference (EMI) signal being able to get inside an enclosed device by coupling into external cables.

The simulations were carried out at a frequency of 1 GHz with 1 V on the antenna for a variety of antenna orientations, ranges and box sizes. Table G.3 summarises the results obtained for three antenna orientations at a range of 0.3 m (1 wavelength at 1 GHz). The magnitude of the load currents at both ends are given as well as the maximum differential and common mode current on the line. In order to compare with a typical mobile phone note that multiplication by a factor of about 28 corresponds to 2 W radiated power from the dipole. Compared to the PWTL without the box attached we see that mode conversion has occurred resulting in EMI in the load resistor. The actual current distribution on the line is shown in Figure G.17 compared with that obtained with no box present. This clearly demonstrates the generation of the differential mode

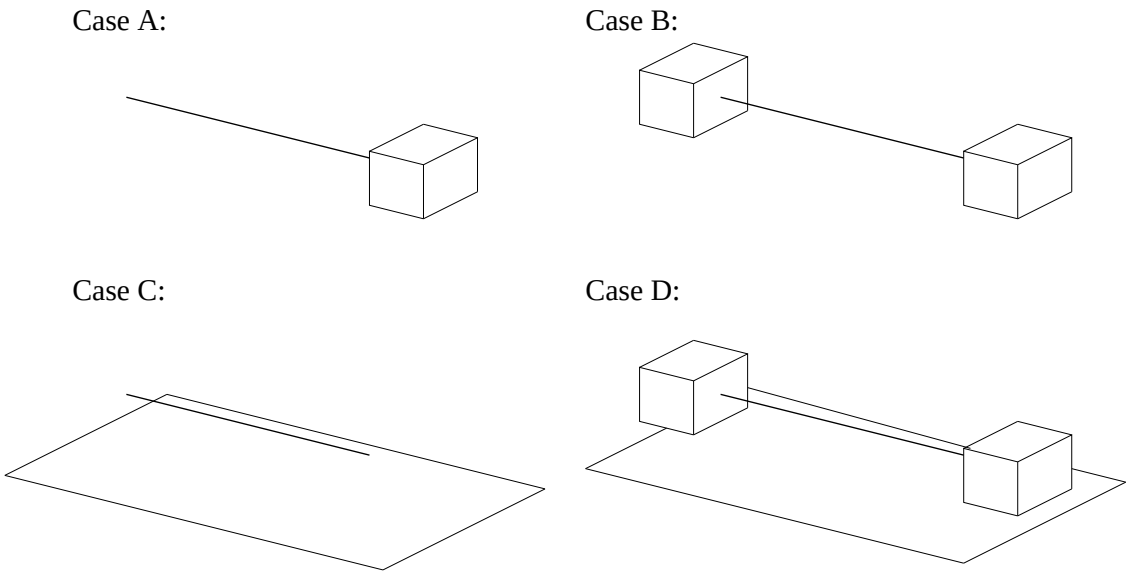

Figure G.16: Configurations investigated for the PWTL model with unbalanced terminations.

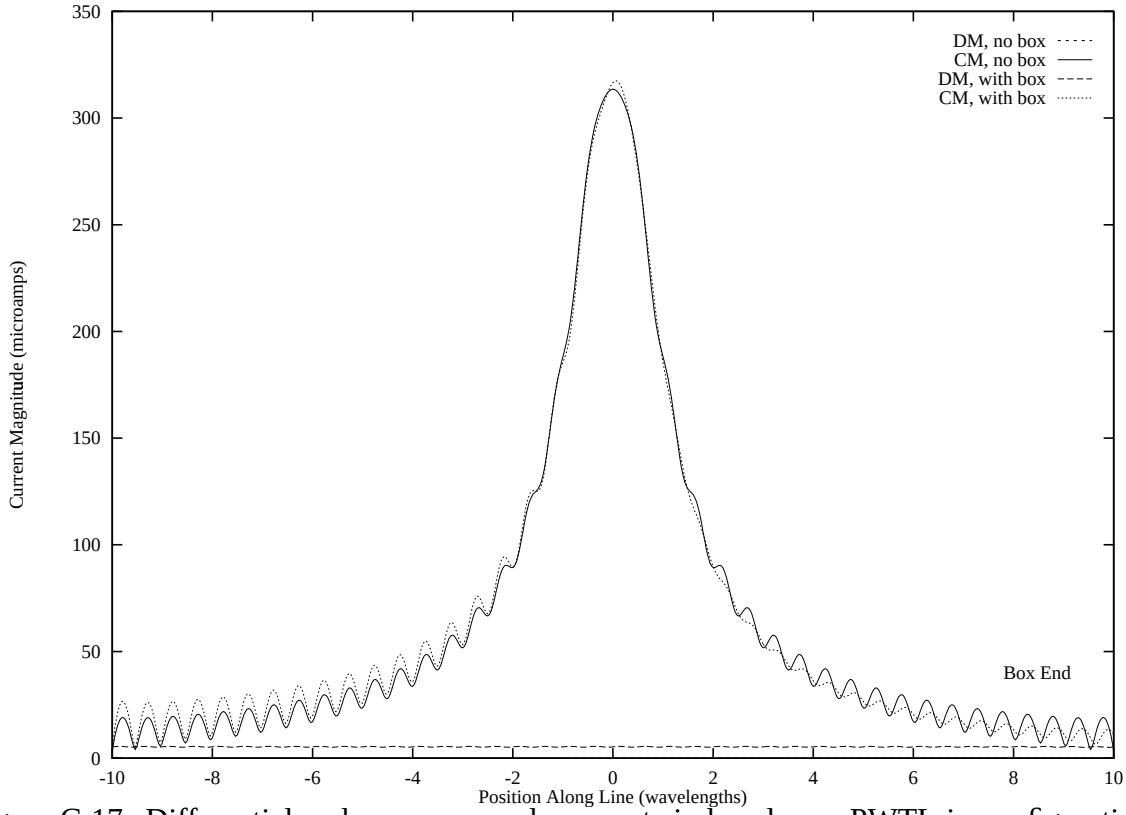

Figure G.17: Differential and common mode currents induced on a PWTL in configuration 6 with and without the box at the right hand end.

Antenna Orientation	Free End Load Current μA	Box End Load Current (μA)	Maximum DM Current (μA)	Maximum CM Current (μA)
3	4.8	4.5	78.8	316
5	9.4	9.2	22.9	12.9
6	5.3	5.1	5.6	317

Table G.3: Summary of results for Case A. The magnitude of the current in each load is given together with the maximum differential-mode (DM) and common-mode (CM) currents on the line.

current by the presence of the box. Note that the differential mode current also propagates to the other end of the line and appears in the load not connected to the box. This highlights the potential risk to shielded devices from EMI due to coupling into external cables.

Results from other configurations show essentially the same form of behaviour. Note that mode conversion in the opposite direction is also possible. For example, with the antenna in configuration 5 the pickup on the PWTL is in the differential mode when the box is not present, however with the box in place we see a common mode component in the current induced on the line.

G.5.6 Case B - Box on both ends of the line

This case shows no important new features compared to case A. It should be noted however that the differential mode current on the line now tends to appear as a standing wave with a high VSWR since both ends of the line now launch a differential mode current wave along the line. The magnitude of the differential mode current tends to be higher than with just one box on the line, but the amount of this current appearing in the load depends on the length of the line - i.e. where in the standing wave pattern the load is located.

G.5.7 Case C - Ground plane

The placing of a perfectly conducting ground plane below the transmission line and dipole antenna has a significant effect on the current induced on the cable. The system can be simulated directly using NEC giving the currents shown in Figure G.18 for configuration 6 with a ground plane 0.8 m below the transmission line. To aid interpretation of the results it is useful to consider the equivalent image problem consisting of the images of both the PWTL and dipole in the ground plane. Since common-mode pickup is usually dominant we can replace the PWTL by a single wire with some effective radius so that the image system contains a new PWTL with a very large wire separation (twice the height of the original PWTL above the ground plane) and two dipole antennas. The nulls in the common-mode current shown in Figure G.18 can then be attributed to the destructive interference of the fields from the two dipoles. Such a configuration can in fact be solved theoretical using the same method as was used for the differential mode currents on a free space PWTL. This method is however incapable of accounting for differential mode currents which can also be induced on the line or caused by mode conversion.

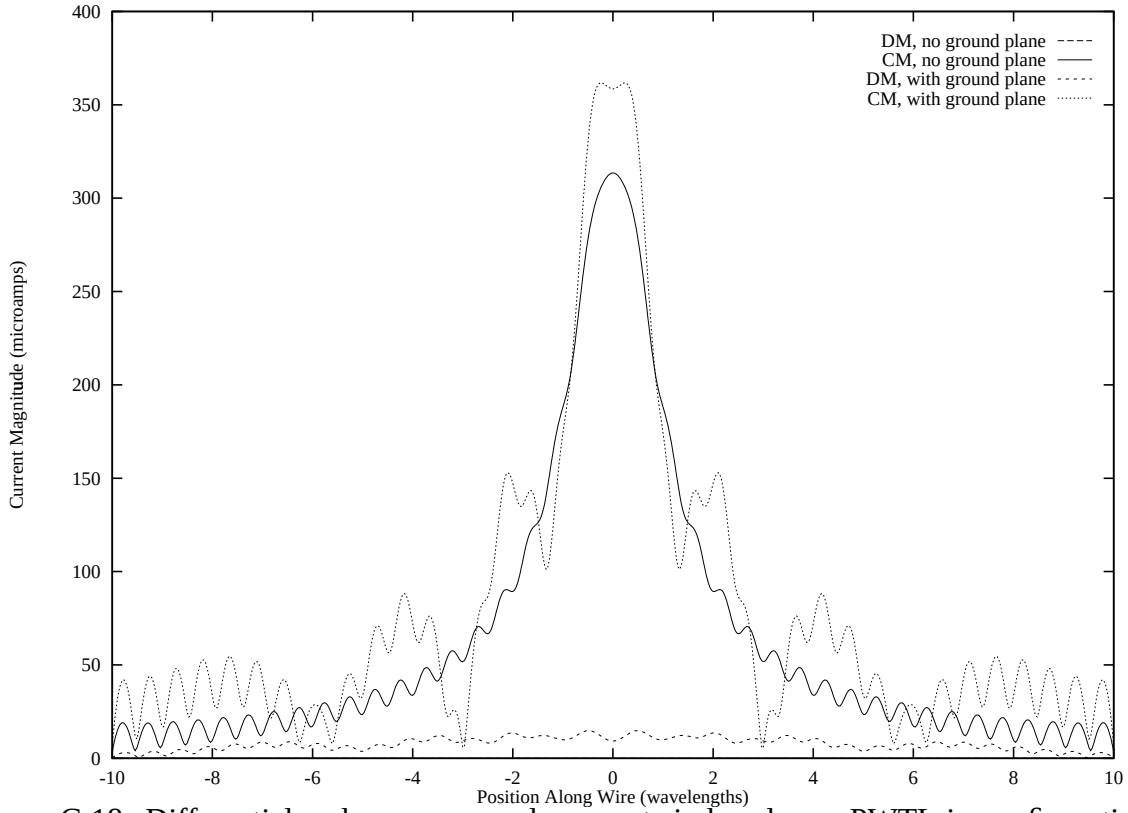

Figure G.18: Differential and common mode currents induced on a PWTL in configuration 6 with and without a ground plane 0.8 m below the line.

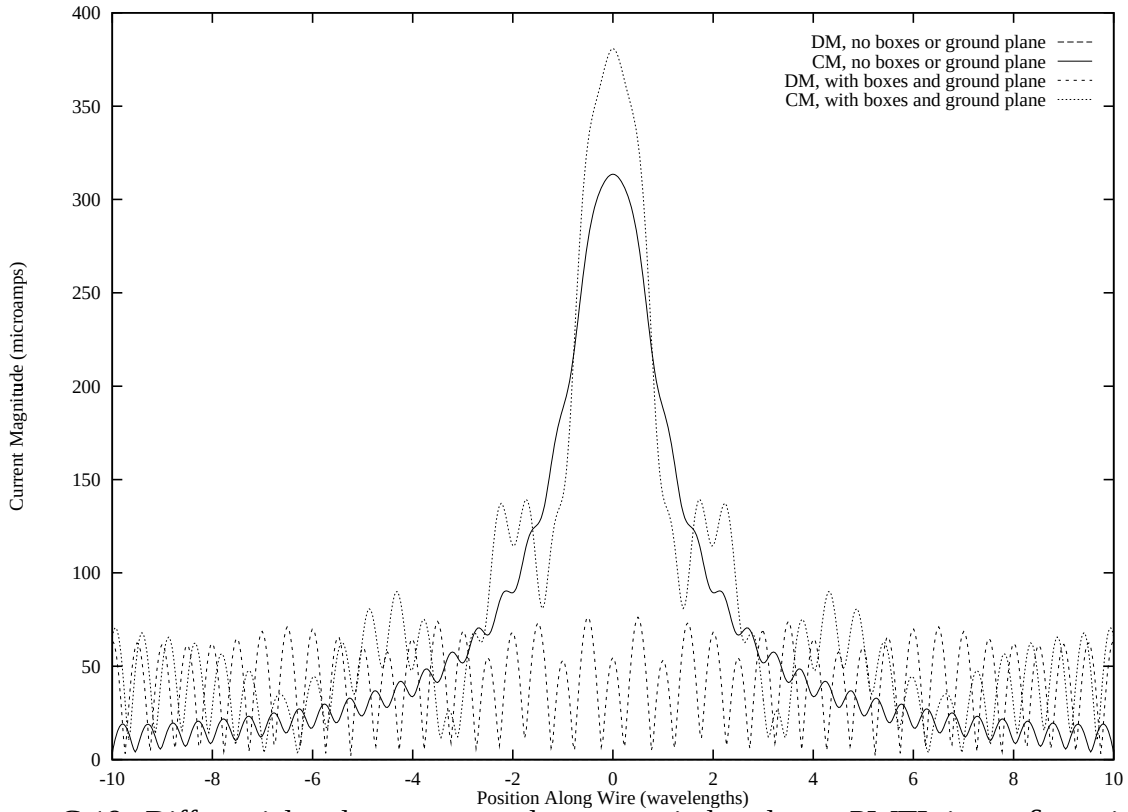

Figure G.19: Differential and common mode currents induced on a PWTL in configuration 6 with and without the box at the right hand end and a ground plane 0.8 m below the line.

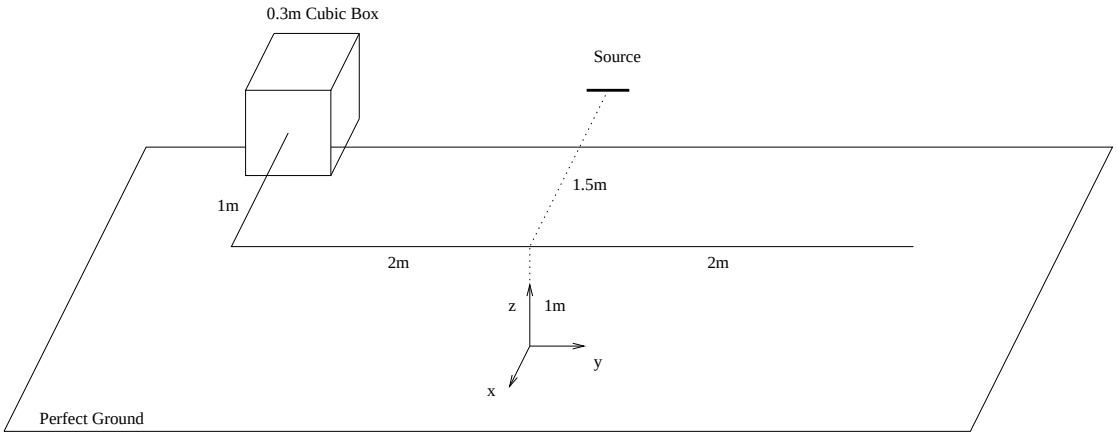

Figure G.20: Typical scenario.

G.5.8 Case D - Ground plane and box on each end of the line

Placing boxes on each end of the line causes mode conversion in much the same way as when the ground plane is not present (see Figure G.19). Note the large differential-mode current (with a high VSWR) produced by the presence of the two boxes, much larger than that which is produced without the ground plane present. This illustrates the importance of reflections from nearby conducting surfaces in determining the threat from EMI coupling into cables.

G.6 Scenario Models

The geometry for a typical scenario is shown in Figure G.20. It consists of a cable of length 5 m running around a corner 1 m above a perfect ground plane. One end of the cable is attached to a 0.3 m cubic box which is modelled as a wire grid. The figure shows a single dipole source at a range of 1.5 m from the midpoint of the longest part of the cable.

Initial simulations were carried out with NEC using a wire grid model for the box. Other simulations were done with CONCEPT using both a wire grid and surface patches. This allowed the effect of modelling approximations to be assessed. The common-mode current induced on the surface of the cable (which is insensitive to the type of cable used) is shown in Figure G.21 and Figure G.22. As can be seen good agreement between NEC and CONCEPT is obtained both with the wire-grid and surface patch models.

Transfer functions were then calculated for the same geometry but with three sources distributed as shown in Figure G.23. Source 1 is the same as in Figure G.20. This was done using the wire-grid model in NEC for frequencies in the GSM band 880-920 MHz. For each source the simulation is run over the frequency range of interest with unit voltage on the source. The other sources are short circuited and not excited. The load current and hence voltage in each load (two in this case) are determined. In the following T_{ji} will be used to denote the voltage induced in load j due to the signal from source i, i.e. it is a voltage transfer function through the system from the mobile source to the victim device. The results presented here are for a 115 Ω unshielded parallel-wire transmission line with matched loads at each end. This is expected to be a worst case for interference pickup amongst the cables considered.

The results for the two loads are shown in Figure G.24 and Figure G.25. The variation of the transfer function with frequency shows that a frequency resolution of around 2 MHz at 1 GHz

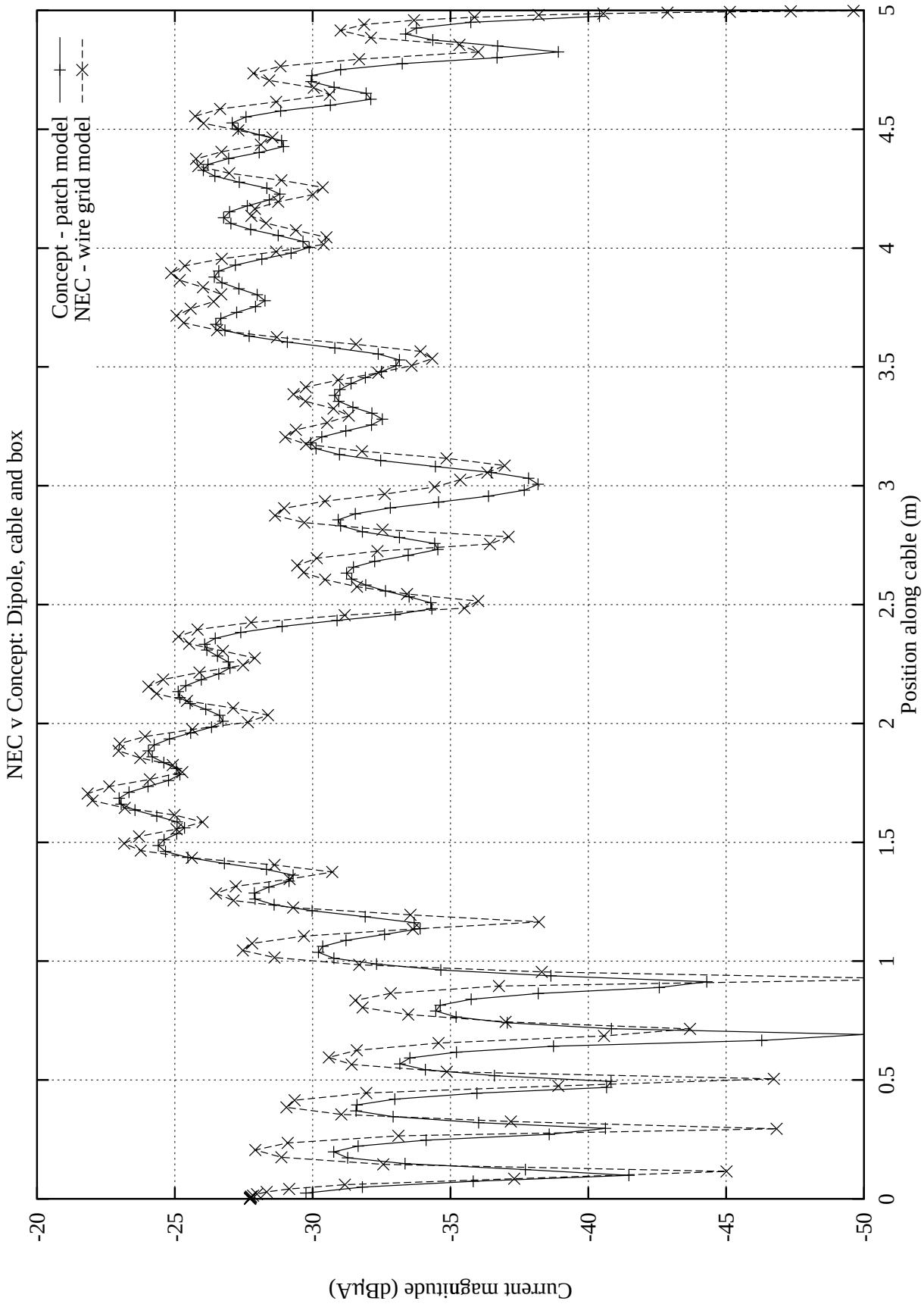

Figure G.21: Magnitude of common-mode current induced on cable.

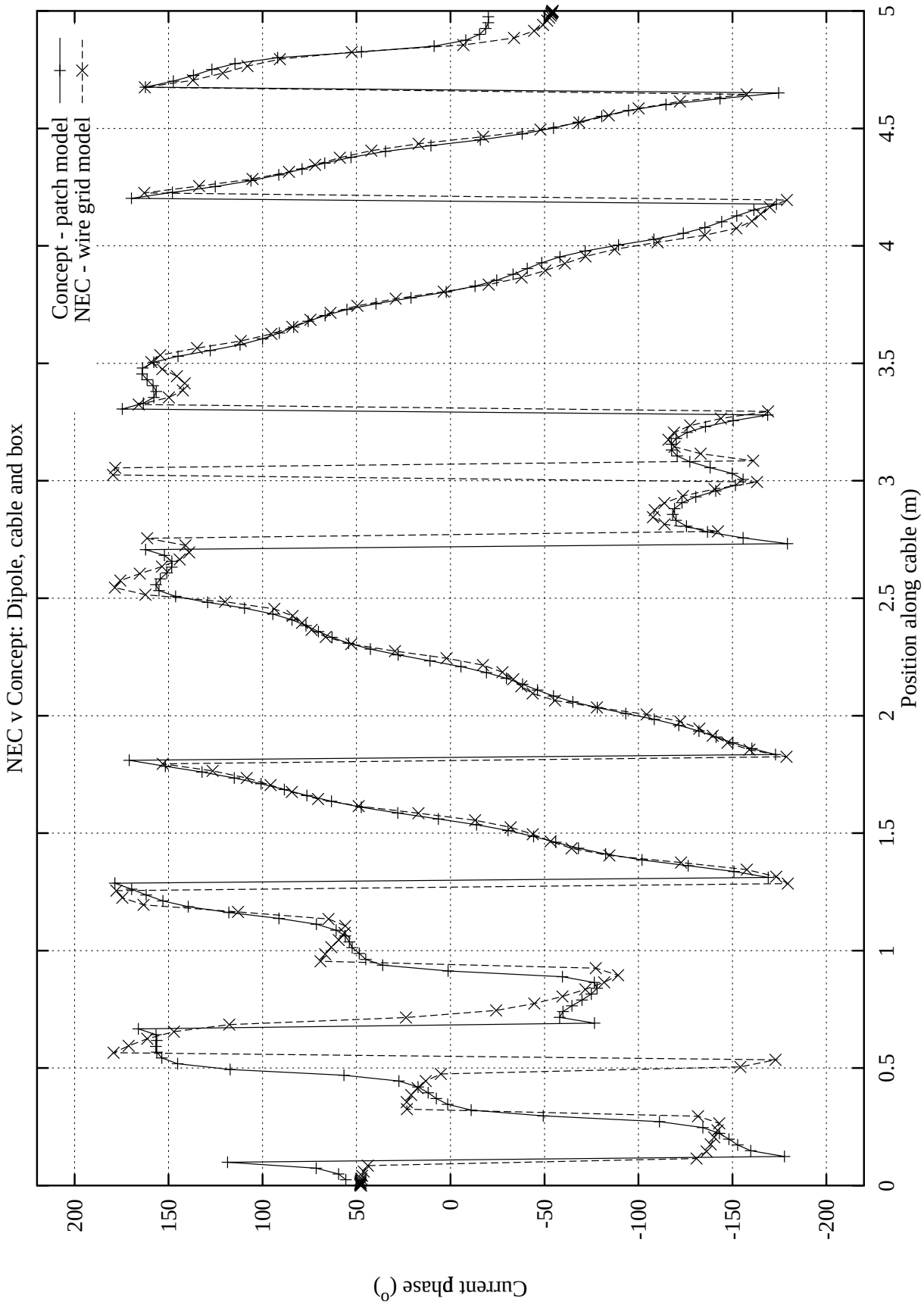

Figure G.22: Phase of common-mode current induced on cable.

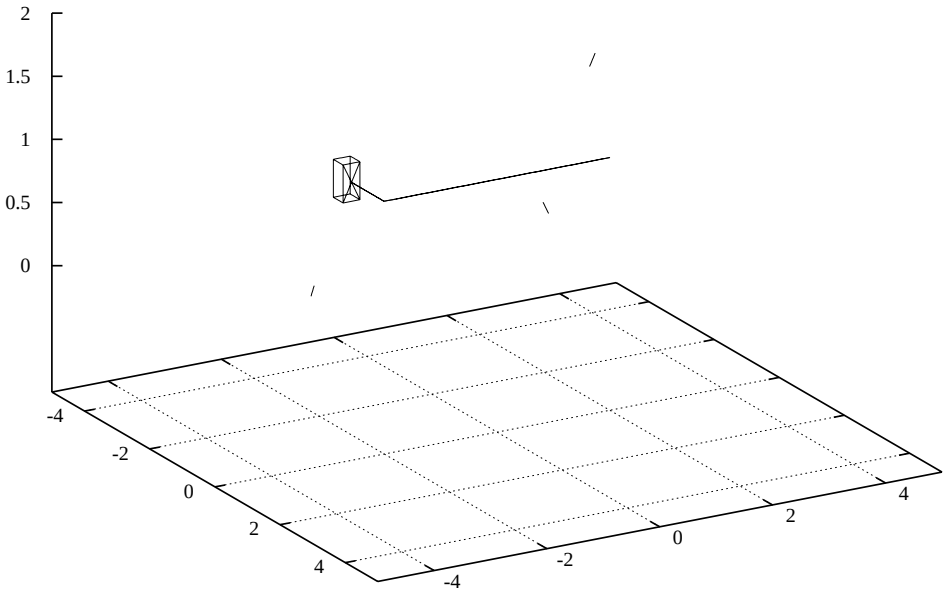

Figure G.23: Location of sources for transfer function calculation.

is appropriate for the EM simulations. Note that for the dipole sources used in the simulations an input voltage of around 28 V leads to a radiated power of about 2 W. This is the maximum radiated power for most hand-held phones. This shows that signals with magnitudes of the order of 50 mV are possible for the given geometry.

G.7 Cables As Distributed Antennas

From the perspective of pickup of interference a cable can be considered as a distributed antenna. The signal generated at the load terminals is the superposition of many elemental sources distributed along the cable. Considering the input terminals of a radio source and the output terminals of a cable as a radio propagation channel the effect of the distributed coupling of energy into the cable is similar to multipath propagation in a normal radio channel. This results in time dispersion of the signal from the radio source as observed in the cable loads. The amount of dispersion is dependent on the relative geometry of the source and cable and the cable propagation parameters.

Figure G.26 illustrates a single radio source at position $\mathbf{r}_j$ coupling to a cable which runs from $\mathbf{r}_S$ to $\mathbf{r}_L$ by some path. The total dispersion time, T_D, of the signal observed in the load at $\mathbf{r}_S$ can be written as:

$$\begin{aligned} T_D &= \left[\frac{|\mathbf{r}_L - \mathbf{r}_j|}{c} + \frac{L}{v_p}\right] - \frac{|\mathbf{r}_S - \mathbf{r}_j|}{c} \\ &= \frac{|\mathbf{r}_L - \mathbf{r}_j| - |\mathbf{r}_S - \mathbf{r}_j|}{c} + \frac{L}{v_p} \end{aligned} \tag{G.49}$$

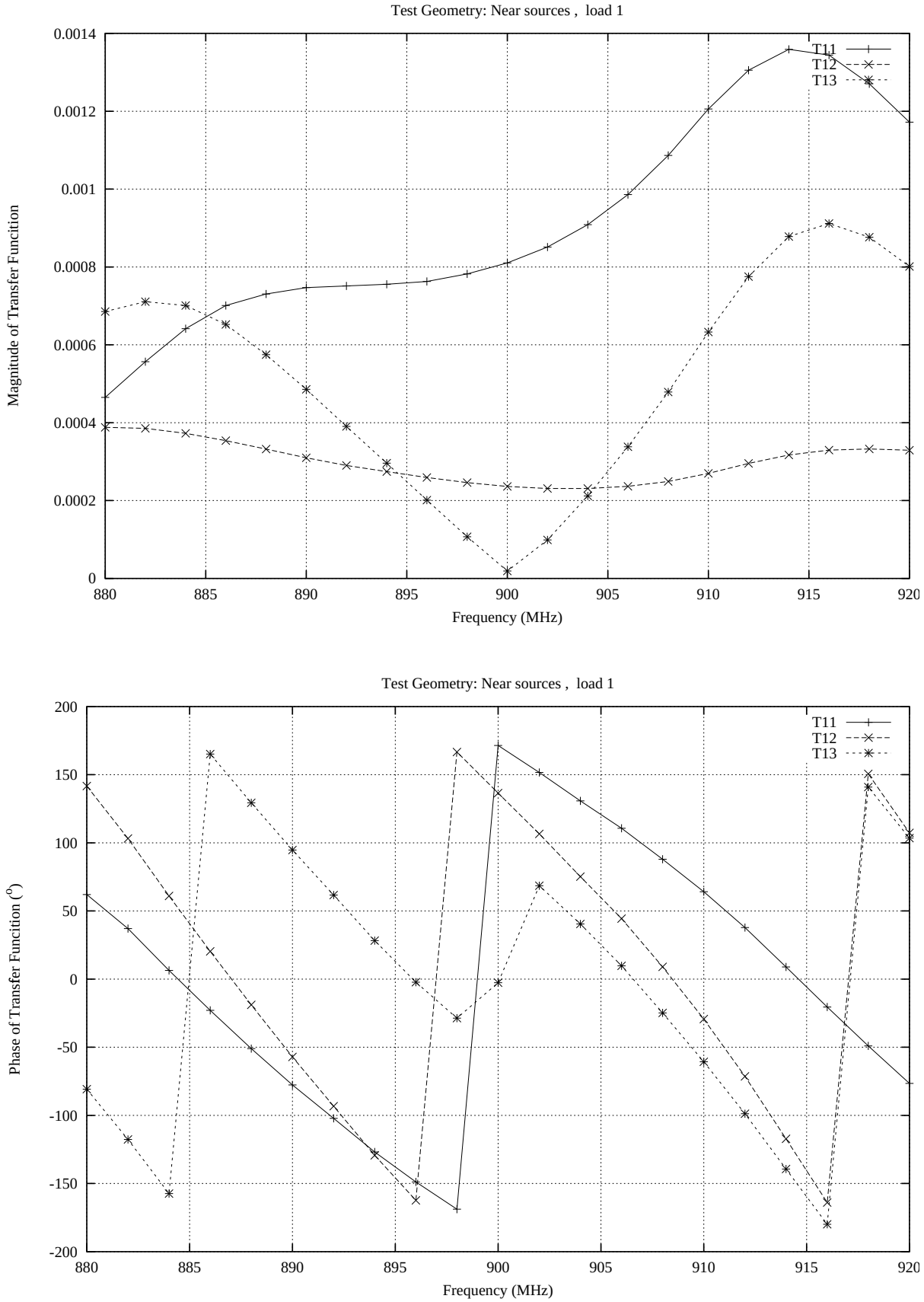

Figure G.24: The magnitude and phase of the transfer function for load 1.

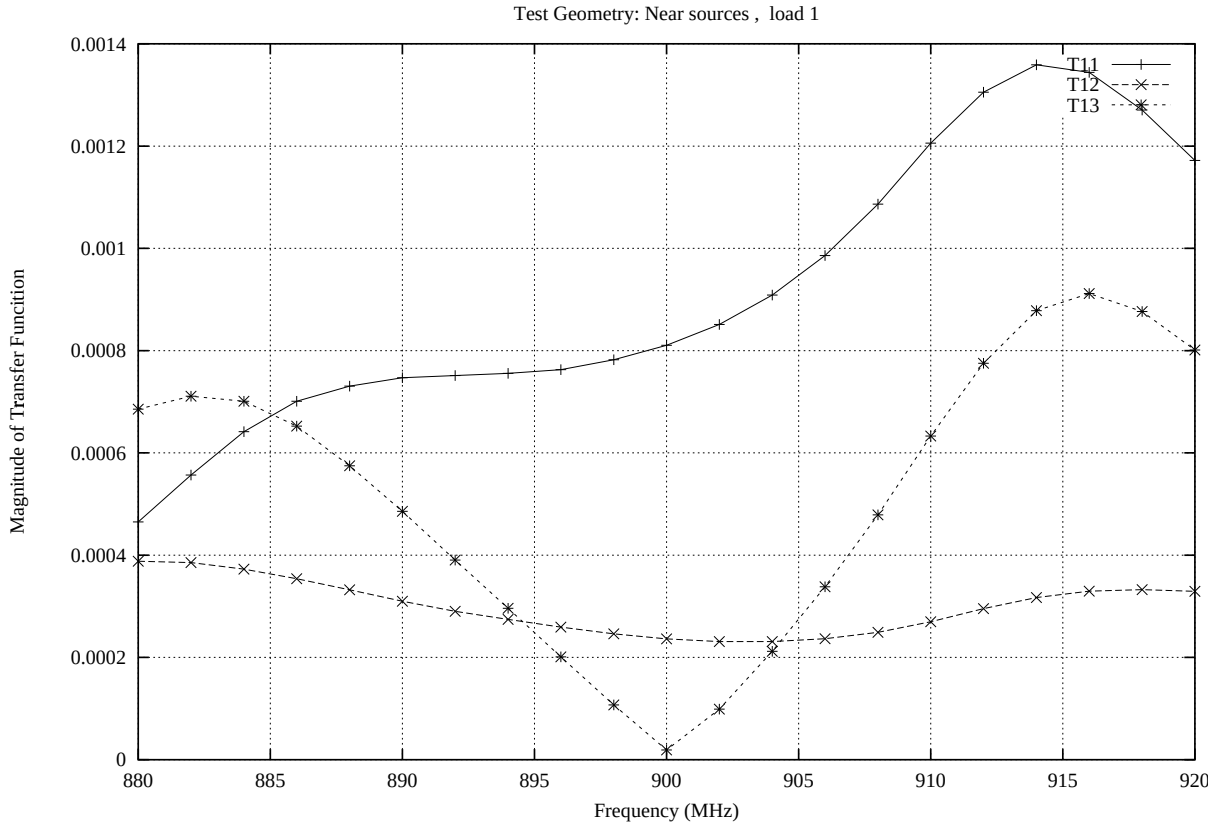

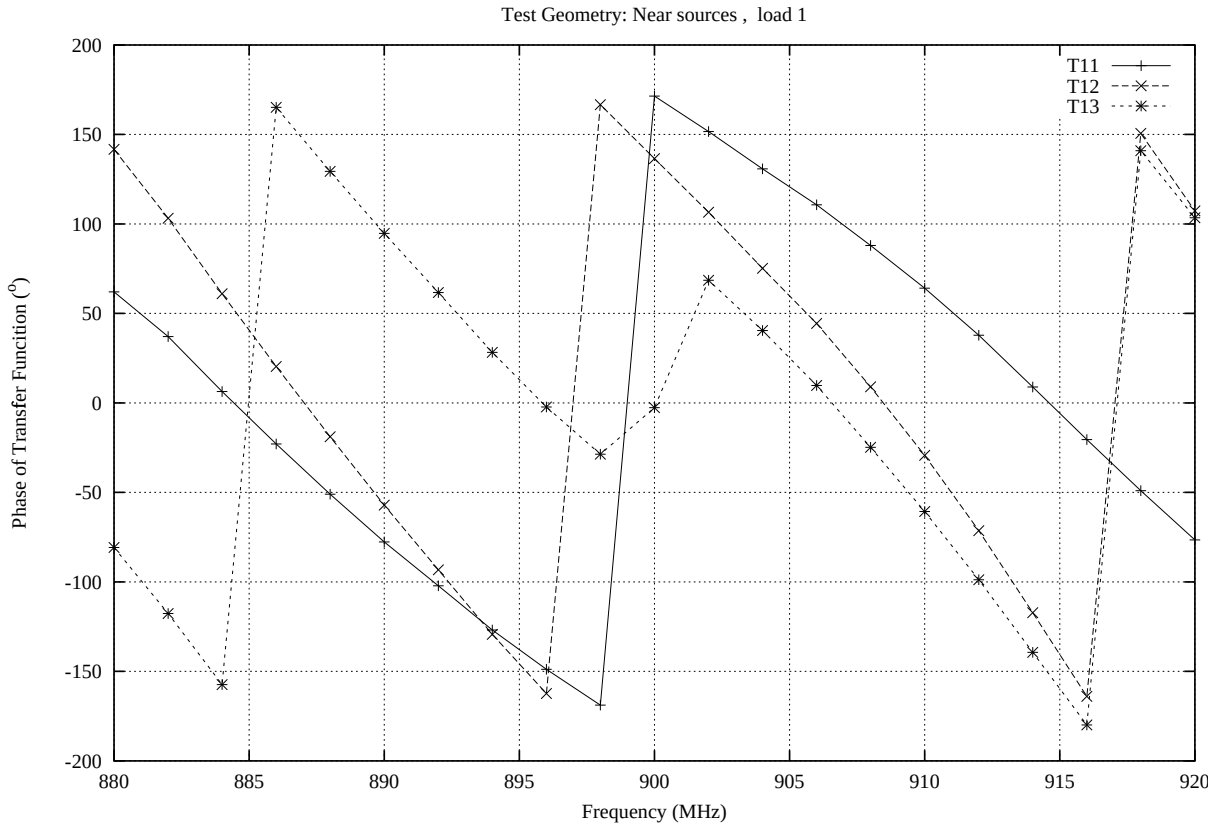

Figure G.25: The magnitude and phase of the transfer function for load 2.

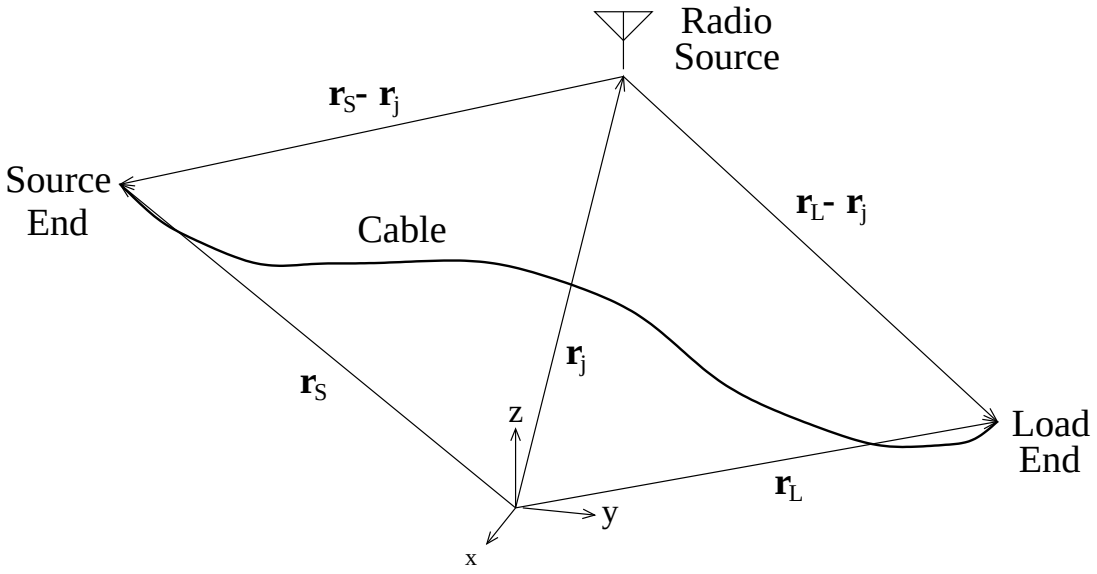

Figure G.26: Time dispersion due to distributed pickup.

where c and v_p are the velocity of light in free space and on the cable respectively and L is the total cable length. Since

$$0 \leq |\mathbf{r}_L - \mathbf{r}_j| - |\mathbf{r}_S - \mathbf{r}_j| \leq L \tag{G.50}$$

$$\frac{L}{v_p} \geq \frac{L}{c} \tag{G.51}$$

the time dispersion can be bounded by

$$\frac{L}{v_p} \leq T_D \leq \frac{2L}{v_p}. \tag{G.52}$$

Hence the coherence bandwidth of the system is

$$\begin{aligned} f_{\text{coherence}} \overset{\text{def}}{\equiv} \frac{1}{T_D} &= \frac{v_p}{2L} \\ &\approx \frac{c}{2L}. \end{aligned} \tag{G.53}$$

The interaction of a radio source with the cable can only be considered narrow band if the bandwidth of the source is much smaller than this coherence bandwidth, that is if

$$f_{\text{source}} << f_{\text{coherence}}. \tag{G.54}$$

Table G.4 gives the maximum cable lengths for which some common mobile telecommunication systems can be regarded as narrow band EMC threats. Cable lengths for both individual sources and the system as a whole are given. These lengths are estimated assuming that the system can be regarded as narrow band if $f_{\text{source}} \leq f_{\text{coherence}}/10$.

All of the *systems* must therefore be considered wide band threats to cables over about half a meter in length and single UMTS sources will be wide band threats to cables of the order of 3 m in length.

System	Channel Bandwidth (kHz)	System Bandwidth (MHz)	Channel Coherence Length (m)	System Coherence Length (m)
TETRA	25	20	600	0.75
GSM900	200	25	75	0.60
PCN1800	200	40	75	0.38
DECT	1728	18	8.7	0.83
UMTS	5000	20	3	0.75

Table G.4: Maximum length of cable for coherent load signals.

G.8 Time Domain Models

G.8.1 FDTD Solution

The excited transmission line equations (G.6) and (G.7) in the time domain are

$$\frac{\partial v^t(\xi,t)}{\partial \xi} + l\frac{\partial i(\xi,t)}{\partial t} + ri(\xi,t) = v_F(\xi,t) \quad \text{(G.55)}$$

$$\frac{\partial i(\xi,t)}{\partial \xi} + c\frac{\partial v^t(\xi,t)}{\partial t} + gv^t(\xi,t) = i_F(\xi,t) \quad \text{(G.56)}$$

where we have assumed that the loss terms r and g are independent of frequency. This approximation can be removed at the expense of complex convolution terms in the FDTD equations [6]. The excitation terms are now

$$v_F(\xi,t) = \frac{\partial}{\partial t}\int_0^s B_v^i(\mathbf{r},t)\,du \quad \text{(G.57)}$$

$$i_F(\xi,t) = -\left(g + c\frac{\partial}{\partial t}\right)\int_0^s E_u^i(\mathbf{r},t)\,du. \quad \text{(G.58)}$$

The numerical solution of these equations can be made more efficient by using the scattered field approach [5] in which the total voltage v^t is replaced by the scattered voltage v^s defined by

$$v^t(\xi,t) = v^s(\xi,t) + v^i(\xi,t) \quad \text{(G.59)}$$

$$= v^s(\xi,t) - \int_0^s E_u^i(u,0,\xi,t)\,du \quad \text{(G.60)}$$

where $v^i(t)$ is the incident voltage. The coupled transmission line equations for the scattered voltage and current can then be written

$$\frac{\partial v^s(\xi,t)}{\partial \xi} + l\frac{\partial i(\xi,t)}{\partial t} + ri(\xi,t) = v_F^s(\xi,t) \quad \text{(G.61)}$$

$$\frac{\partial i(\xi,t)}{\partial \xi} + c\frac{\partial v^s(\xi,t)}{\partial t} + gv^s(\xi,t) = 0 \quad \text{(G.62)}$$

where the excitation term for the first equation is

$$v_F^s(\xi,t) = E_\xi^i(s,0,\xi,t) - E_\xi^i(0,0,\xi,t). \quad \text{(G.63)}$$

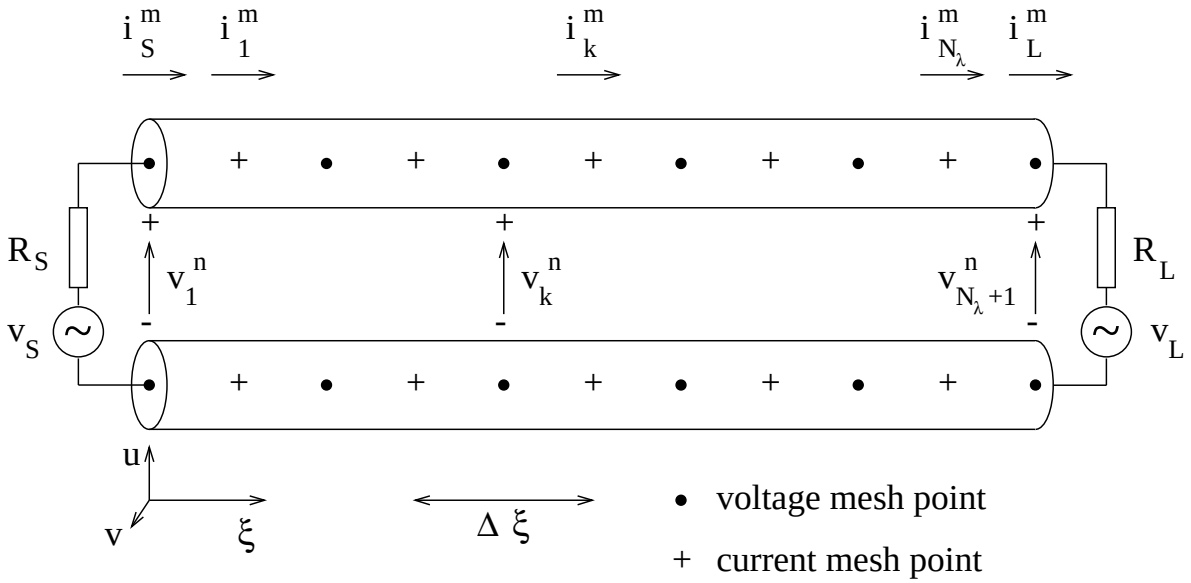

Figure G.27: Space time discretisation of the transmission line using the leapfrog method.

There is no excitation term for the second equation in this formulation which significantly reduces the computational time needed to solve the equations providing the total voltage is only observed at a few points along the cable.

The equations are discretised by dividing the cable into uniform interlaced current and voltage meshes to give second order accuracy (see Figure G.27). The current is calculated at N_ξ points $\xi = (k-1/2)/\Delta\xi$ $(k = 1, \ldots, N_\xi)$ where $\Delta\xi = L/N_\xi$ and the voltage at $N_\xi + 1$ points $\xi = (k-1)/\Delta\xi$ $(k = 1, \ldots, N_\xi + 1)$. Time is similarly discretised into N_t segments of length Δt.

Defining the voltages and currents by

$$v_k^n = v^s\left((k-1)\Delta\xi, n\Delta t\right) \quad (k = 1, \ldots, N_\xi + 1) \tag{G.64}$$

$$i_k^n = i\left((k-1/2)\Delta\xi, n\Delta t\right) \quad (k = 1, \ldots, N_\xi) \tag{G.65}$$

$$v_{F,k}^n = v_F^s\left((k-1)\Delta\xi, n\Delta t\right) \quad (k = 1, \ldots, N_\xi + 1) \tag{G.66}$$

the transmission line equations can be written

$$\left(\frac{l\Delta\xi}{\Delta t} + \frac{r\Delta\xi}{2}\right) i_k^{n+3/2} = \left(\frac{l\Delta\xi}{\Delta t} - \frac{r\Delta\xi}{2}\right) i_k^{n+1/2} - v_{k+1}^{n+1} + v_k^{n+1} + \frac{\Delta\xi}{2}(v_{F,k}^{n+3/2} + v_{F,k}^{n+1/2}) \tag{G.67}$$

$$\left(\frac{c\Delta\xi}{\Delta t} + \frac{g\Delta\xi}{2}\right) v_k^{n+1} = \left(\frac{c\Delta\xi}{\Delta t} - \frac{g\Delta\xi}{2}\right) v_k^n - i_k^{n+1/2} + i_{k-1}^{n+1/2} \tag{G.68}$$

using second order central differences [6]. To incorporate the terminal constraints the transmission line equations must be discretised differently at the source and load points since the boundary conditions relate the current and voltage at the same place and time. When this is

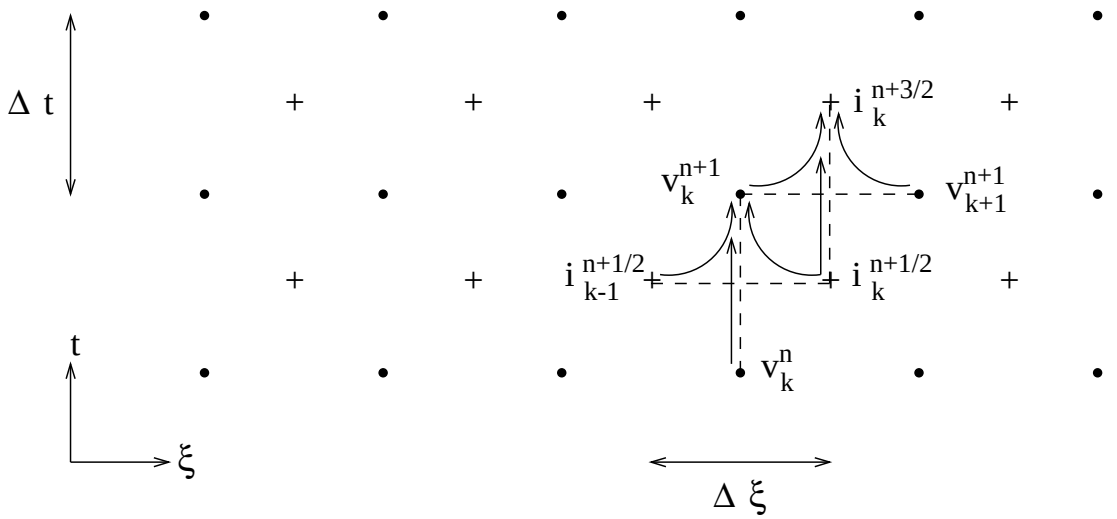

Figure G.28: Update chart for the voltage and current meshes.

done for the Thévenin source and load constraints

$$\begin{aligned} v_1^t(t) &= v_S^s(t) + v_S^i(t) \\ &= v_S(t) - R_S i_S(t) \qquad \text{(G.69)} \\ v_{N_\xi+1}^t(t) &= v_L^s(t) + v_L^i(t) \\ &= v_L(t) + R_L i_L(t) \qquad \text{(G.70)} \end{aligned}$$

we get the following equations for updating the voltage at the end points:

$$\begin{aligned} \left(\frac{R_S c\Delta\xi}{2\Delta t} + \frac{R_S g\Delta\xi}{4} + \frac{1}{2}\right) v_1^{n+1} &= \left(\frac{R_S c\Delta\xi}{2\Delta t} - \frac{R_S g\Delta\xi}{4} - \frac{1}{2}\right) v_1^n \\ &- R_S i_1^{n+1/2} + \frac{1}{2}\left(v_S^{n+1} + v_S^n\right) \\ &- \frac{1}{2}\left(v_S^{i,n+1} + v_S^{i,n}\right) \\ &+ \frac{R_S\Delta\xi}{4}\left(i_{F,1}^{n+1} + i_{F,1}^n\right) \qquad \text{(G.71)} \\ \left(\frac{R_L c\Delta\xi}{2\Delta t} + \frac{R_L g\Delta\xi}{4} + \frac{1}{2}\right) v_{N_\xi+1}^{n+1} &= \left(\frac{R_L c\Delta\xi}{2\Delta t} - \frac{R_L g\Delta\xi}{4} - \frac{1}{2}\right) v_{N_\xi+1}^n \\ &+ R_L i_{N_\xi}^{n+1/2} + \frac{1}{2}\left(v_L^{n+1} + v_L^n\right) \\ &- \frac{1}{2}\left(v_L^{i,n+1} + v_L^{i,n}\right) \\ &+ \frac{R_L\Delta\xi}{4}\left(i_{F,N_\xi+1}^{n+1} + i_{F,N_\xi+1}^n\right) \qquad \text{(G.72)} \end{aligned}$$

where

$$\begin{aligned} v_S^{i,n} &= v^i\left(0, n\Delta t\right) \qquad \text{(G.73)} \\ v_L^{i,n} &= v^i\left(L, n\Delta t\right) \qquad \text{(G.74)} \end{aligned}$$

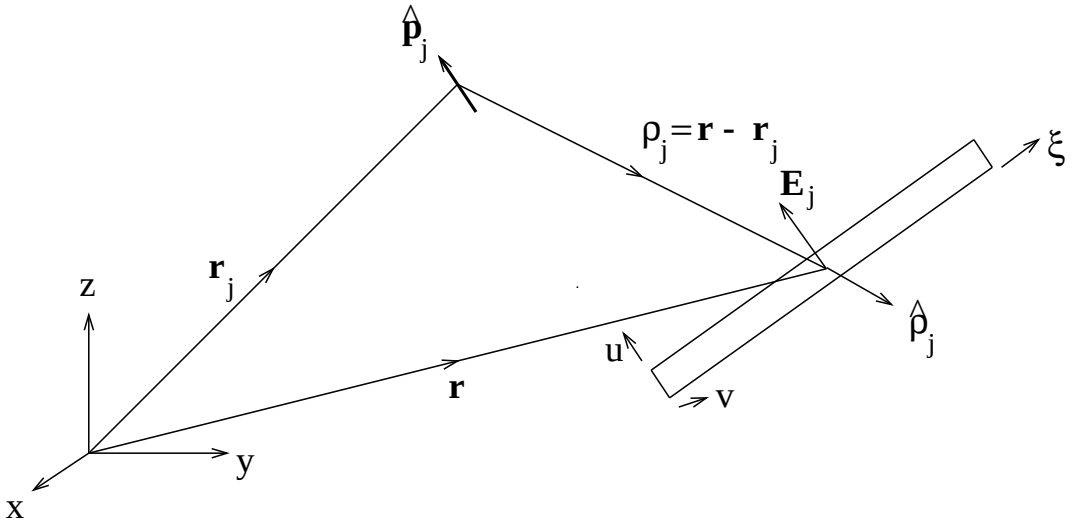

Figure G.29: Coordinate systems for combined transmission line and GMSK source mode.

are the incident voltages at the source and load points.

The time and space meshes must satisfy the Courant condition [9]

$$\Delta t \leq \frac{\Delta \xi}{v_p}, \tag{G.75}$$

where v_p is the phase velocity of the transmission line, in order for the solution to be stable. In fact it can be shown that for the 'magic' time step $\Delta t = \Delta \xi / v_p$ the FDTD solution is an exact representation of the solution of the coupled transmission line equations [7]. For an accurate solution the segment length $\Delta \xi$ on the transmission line must be chosen to be a small fraction of a wavelength at the highest frequency of the excitation fields (typically $\Delta \xi = \lambda/10$).

This FDTD approach can be used for predicting the statistics of EMI in cable loads from various sources. Note however that unlike the frequency domain moment method models this FDTD model is unable to account for common mode currents.

G.8.2 Interfacing To A GMSK Phase Constructor

The GMSK phase constructor discussed in Appendix I was interfaced to the FDTD model of the transmission line. Figure G.29 shows the coordinate systems used in the combined model. For interfacing to the transmission line FDTD model the GSM sources are modelled by

$$\mathbf{E}_j(\mathbf{r}, t) = \frac{\sqrt{90 P_j}}{\mid \mathbf{r} - \mathbf{r}_j \mid} \cdot s_j \left(t - \frac{1}{c} \mid \mathbf{r} - \mathbf{r}_j \mid \right) \mathbf{e}_j(\hat{\mathbf{p}}_j, \hat{\boldsymbol{\rho}}_j) \tag{G.76}$$

$$s_j(t) = p(t) \cos(\omega_j t + \theta(\vec{d}, t) + \theta_{j0}) \tag{G.77}$$

where

$$\boldsymbol{\rho}_j = \mathbf{r} - \mathbf{r}_j \tag{G.78}$$

$$\hat{\boldsymbol{\rho}}_j = \frac{\mathbf{r} - \mathbf{r}_j}{\mid \mathbf{r} - \mathbf{r}_j \mid} \tag{G.79}$$

$$\mathbf{e}_j(\hat{\mathbf{p}}_j, \hat{\boldsymbol{\rho}}_j) = \hat{\mathbf{p}}_j - (\hat{\mathbf{p}}_j \cdot \hat{\boldsymbol{\rho}}_j) \hat{\boldsymbol{\rho}}_j. \tag{G.80}$$

and $\hat{\mathbf{p}}_j$ is the polarisation vector of source j. Note that here we are using the non-isotropic polarisation term (G.80) for a infinitesimal dipole which has a gain of 1.5. Hence the factor 60 used in the power normalisation of the isotropic model in Appendix I is replaced by $60 \times 1.5 = 90$. We have also included a power ramping factor $p(t)$ for the TDMA burst which is taken to be

$$p(t) = \frac{1}{T_r}\text{rect}\left(\frac{t}{T_r}\right) \otimes h_{\text{B}}(t) \tag{G.81}$$

where $T_r = 565\,\mu$s and $h_{\text{B}}(t)$ is the impulse response of a second order Bessel filter

$$h_{\text{B}}(t) = \begin{cases} 0 & t < 0 \\ 4\omega_0 \sin \omega_0 t e^{-at} & t > 0 \end{cases} \tag{G.82}$$

with a cut off frequency $f_b = 52\,$kHz ($\omega_b = 2\pi f_b$, $\omega_0 = \sqrt{3}\omega_b/2$ and $a = 3\omega_b/2$) [10].

Taking the ensemble field from N_P phones as

$$\mathbf{E}(\mathbf{r}, t) = \sum_{j=1}^{N_P} \mathbf{E}_j(\mathbf{r}, t) \tag{G.83}$$

the excitation term for the scattered voltage (G.63) can be written

$$v_F^s(\xi, t) = \sum_{j=1}^{N_P} \left[f_j^s(\xi) s_j(t - g_j^s(\xi)) - f_j^0(\xi) s_j(t - g_j^0(\xi)) \right] \tag{G.84}$$

where

$$f_j^{s,0}(\xi) = \frac{\sqrt{90 P_j}}{|\mathbf{r}_{s,0}(\xi) - \mathbf{r}_j|} \left(\mathbf{e}_j \cdot \hat{\boldsymbol{\xi}} \right) \tag{G.85}$$

$$g_j^{s,0}(\xi) = \frac{1}{c}|\mathbf{r}_{s,0}(\xi) - \mathbf{r}_j| - \frac{1}{c}|\mathbf{r}_j|. \tag{G.86}$$

The vectors $\mathbf{r}_0(\xi)$ and $\mathbf{r}_s(\xi)$ are the positions of the two cable conductors at position ξ along the cable,

$$\mathbf{r}_0(\xi) = (0, 0, \xi) \tag{G.87}$$

$$\mathbf{r}_s(\xi) = (s, 0, \xi), \tag{G.88}$$

in the (u, v, ξ) coordinate system. (G.86) includes a term $\frac{1}{c}|\mathbf{r}_j|$ which ensures that the timeslots are received in synchronisation at the centre of the (x, y, z) coordinate system (the base station). The incident voltage can be approximated by

$$v^i(\xi, t) = -\frac{1}{2} s \sum_{j=1}^{N_P} \left[h_j^s(\xi) s_j(t - g_j^s(\xi)) + h_j^0(\xi) s_j(t - g_j^0(\xi)) \right] \tag{G.89}$$

where

$$h_j^{s,0}(\xi) = \frac{\sqrt{90 P_j}}{|\mathbf{r}_{s,0}(\xi) - \mathbf{r}_j|} \left(\mathbf{e}_j \cdot \hat{\mathbf{u}} \right) \tag{G.90}$$

providing the separation of the two wires is much less than a wavelength.

This model was implement in C code. The GMSK phase deviation and power ramping term are pre-sampled ten times per bit and stored as a cubic spline coefficients allowing fast calculation of the excitation term and incident voltage in the time marching FDTD algorithm.

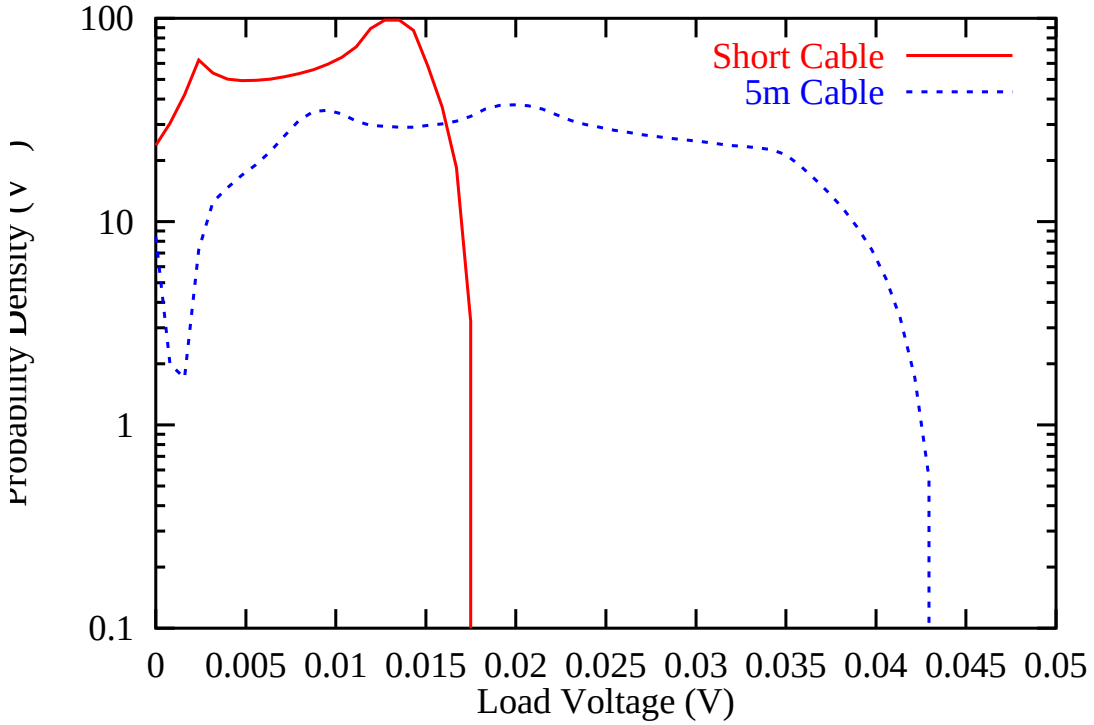

Figure G.30: Statistics of EMI in the load at the end of a matched 115 Ω parallel wire transmission line illuminated by three GSM sources at a range of 1 m on channels 1, 37 and 124. The probability density for a short (0.02 m) cable is compared to that of a 5 m cable.

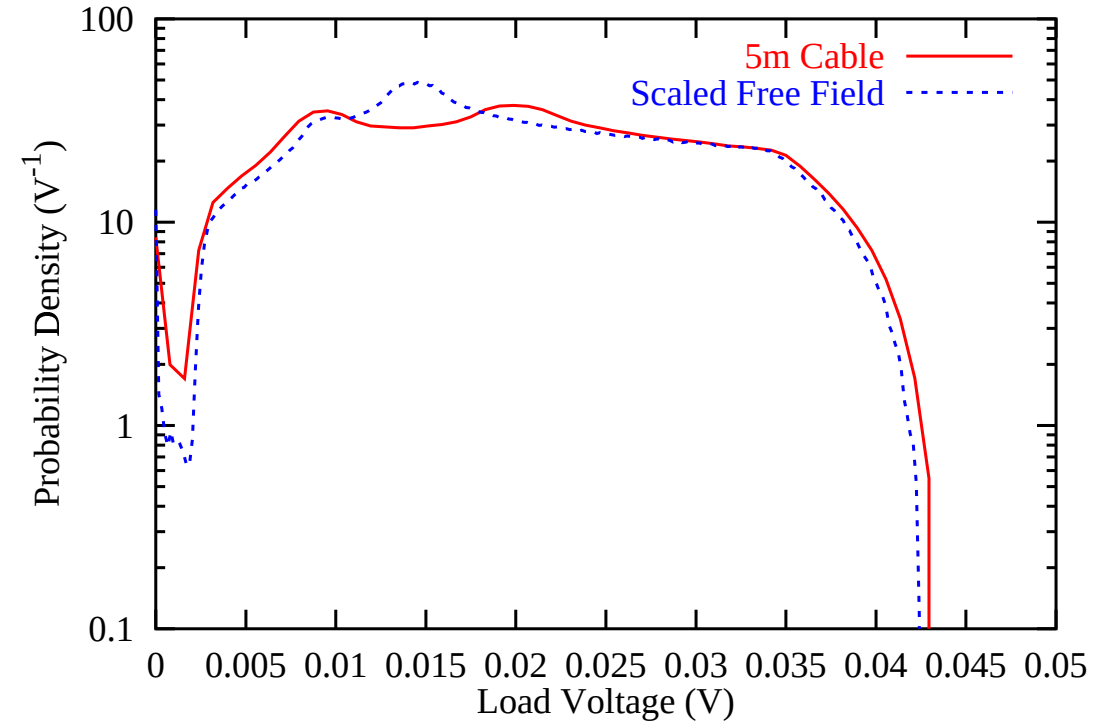

Figure G.31: 5 m cable load voltage PDF compared to the PDF of the free electric field at the centre of cable rescaled to the same magnitude as the load EMI.

G.8.3 Cable Coupling Statistics

Figure G.30 shows the simulated EMI probability density functions (PDFs) for a matched 115 Ω parallel wire cable illuminated by three GSM sources on channels 1, 37, and 124 at a range of 1 m from the cable (see Appendix I.5 for the defintion and interpretation of PDFs). For both the electrically short cable and the 5 m cable the maximum load voltage is determined by the sum of the voltages predicted by the frequency domain transfer function discussed in Section G.3 for each individual source.

Figure G.31 shows the EMI statistics of the 5 m cable again, this time compared to the statistics of the ensemble electric field from the three sources sampled at the centre of the cable. The free field is scaled to roughly the same magnitude as the cable load PDF. This shows that the distributed cable coupling has little effect on the overall statistic of the RF envelope of the ensemble signal.

G.9 Twisted And Shield Cables

Two common methods of reducing the coupling of EMI to cables are the use of twisted cables and shielded cables.

G.9.1 Unshielded Twisted Pair

The basic idea of twisted cables is to provide cancellation of any noise from external fields or crosstalk with other cables by periodically altering the phase of the induced noise. This is accomplished by altering the orientation of the cable conductors with respect to the noise source by an uniform twisting of pairs of signal carrying conductors.

Locally twisted cables are the same as their untwisted counterparts. The uniformity of the cable twist has a large impact on the noise immunity, particularly at high frequencies.

The twisting of cables has little effect on the amount of common mode currents induced - we have already seen that from the point of view of common mode pickup a cable can be treated approximately as a single conductor. If the dominant coupling path is via common mode conversion then twisting cables has little effect.

The modelling of unshielded twisted pair has been considered in two ways:

1. Detailed models for accurate coupling calculations and possibly for use at sensitive interfaces.

2. Less detailed models for coupling and propagation calculations.

For the detailed model of USTP we regard the transmission line as a bifilar helix formed by uniformly twisting a PWTL as illustrated in Figure G.32. For the initial study we again used the 212 Ω PWTL model parameters which have a wire separation of 6 mm since we expect the numerical problems associated with small wire separations to be more important once we introduce twists onto the line. The dielectric coating of USTP is also neglected in these studies since it is expected to produce only second order effects and it is not possible to model within NEC.

It has already been demonstrated with the PWTL that the pickup usually occurs in the common-mode except in certain unusual critical cases. Common mode pickup is insensitive to the detailed structure of the wire, i.e. in this mode the antenna essentially sees a single wire with some effective radius comparable to the overall transverse scale of the transmission line.

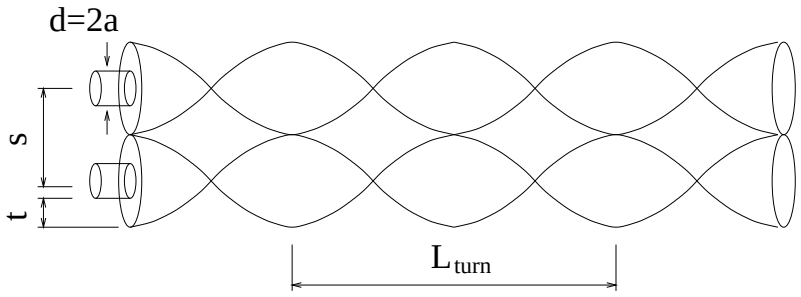

Figure G.32: Geometry of unshielded twisted pair transmission line.

This leads us to consider using a single wire model for the coupling and propagation calculations when we are not interested in the differential mode current (obviously differential mode currents cannot propagate on a single wire). The single wire may be inductively loaded to tune the propagation velocity of the common-mode surface wave to that of a real USTP.

Here we will only consider the detailed model; the single wire model is discussed fully in Section G.9.3. The first thing to note is that introducing a twist on the line immediately forces us to use a finer discretisation of the lines wires since we must model each turn of the USTP using a number of straight wires. This greatly increases the computational power required compared to the PWTL case.

The modelling of the terminations is again critical to achieving reliable results. As with PWTL we require at least 3 segments on the termination wires and this segment length must be "matched" to that used on the line. Dynamic segmentation cannot be implemented on the twisted wire so $\frac{l}{4}$ sections of PWTL were used at each end of the USTP to ensure a smooth variation of segment lengths. The initial work looked at how many wires were needed to model each turn of the USTP and how many segments were needed on each wire to give reasonable convergence for the line currents.

Figure G.33 shows the real part of the current on 0.3 m of USTP using 8 wires per turn and various numbers of segments per wire for a model with a turn length of 10 mm, wire separation of 6 mm and wire diameter of 2 mm. The physical length of the line is measured along the axis of the helix and not along the wire itself and therefore does not represent the electrical length of the line. The results show that reasonable stability can be achieved. Figure G.34 shows a similar plot, but this time varying the number of wires per turn with a single segment on each wire. It should be noted that in this case each curve actually represents the current on a different model of the USTP so we do not expect close agreement. For example, increasing the number of wires per turn in the model increases the electrical length of the line so that more wavelengths fit into the section depicted. (To achieve convergence in the electrical length would require an impractical number of wires on each turn). The variation of the current with the number of wires per turn therefore gives us an indication of how good the straight wire approximation to the helices actually is.

The model was then used to calculate the coupling of a dipole field into the transmission line as was done for the PWTL. Figure G.35 shows the pickup on a 6 λ length of USTP from a dipole in orientation 6 at a range of 1 λ. The behaviour is essentially the same as with the PWTL, however the magnitude of the current is somewhat lower. The results obtained so far suggest that a single wire model will give acceptable results for the common mode pickup on USTP.

The initial work on USTP used unrealistic cable parameters to alleviate modelling diffi-

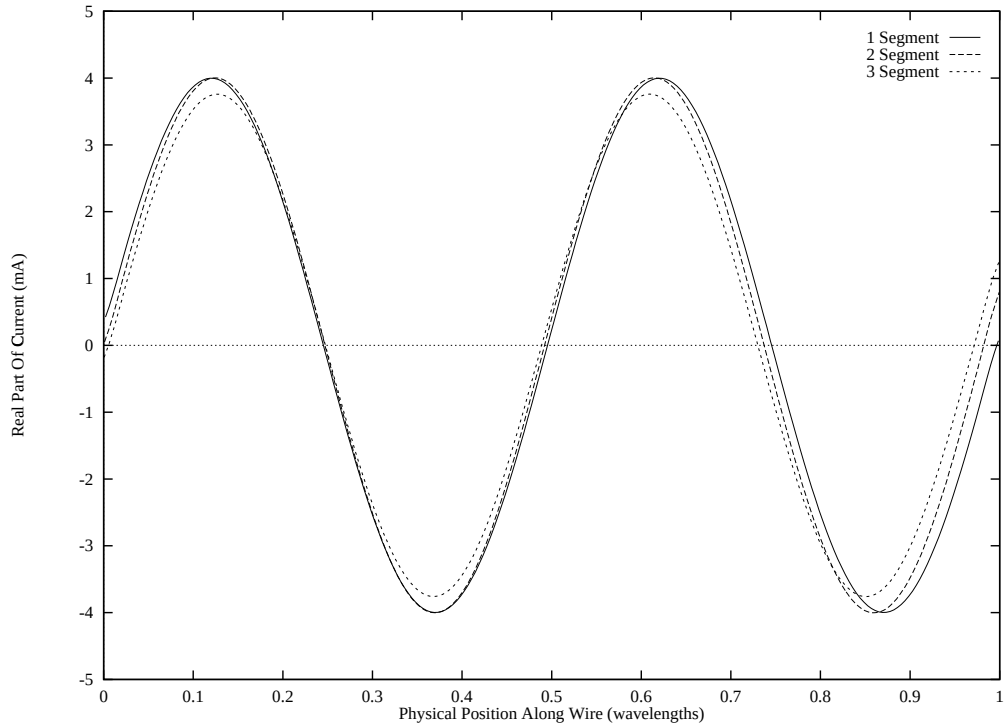

Figure G.33: Real part of the current on a 1 λ section of USTP using 8 wires per turn as a function of the number of segments per wire (turn length 10 mm, wire separation 6 mm, wire radius 1 mm).

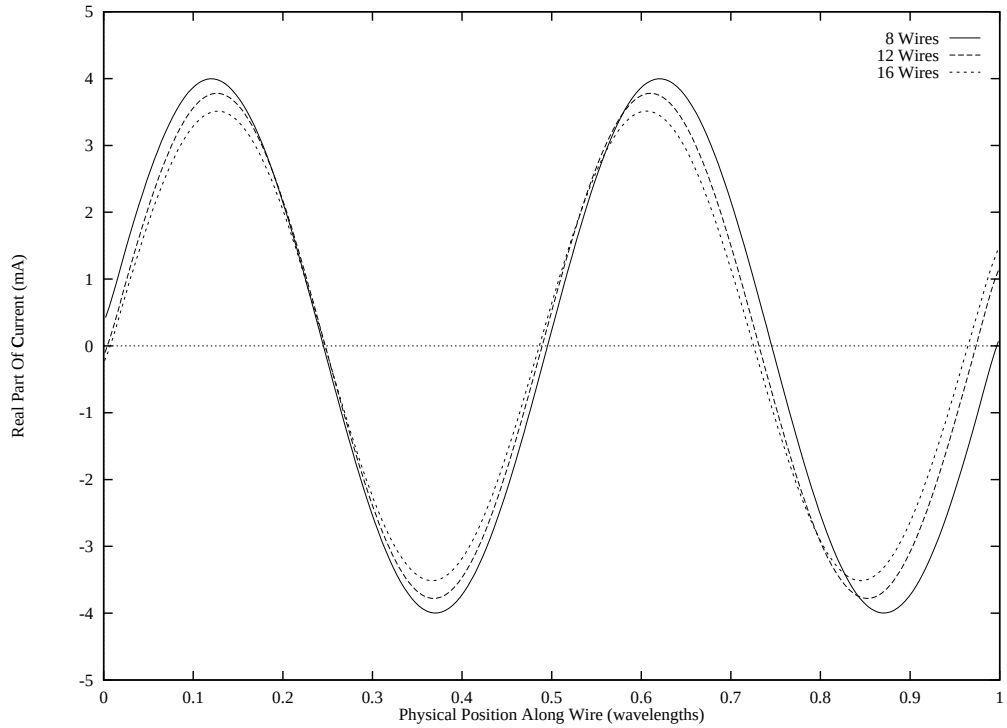

Figure G.34: .Real part of the current on a 1 λ section of USTP using 1 segment per wire as a function of the number of wires per turn (turn length 10 mm, wire separation 6 mm, wire radius 1 mm).

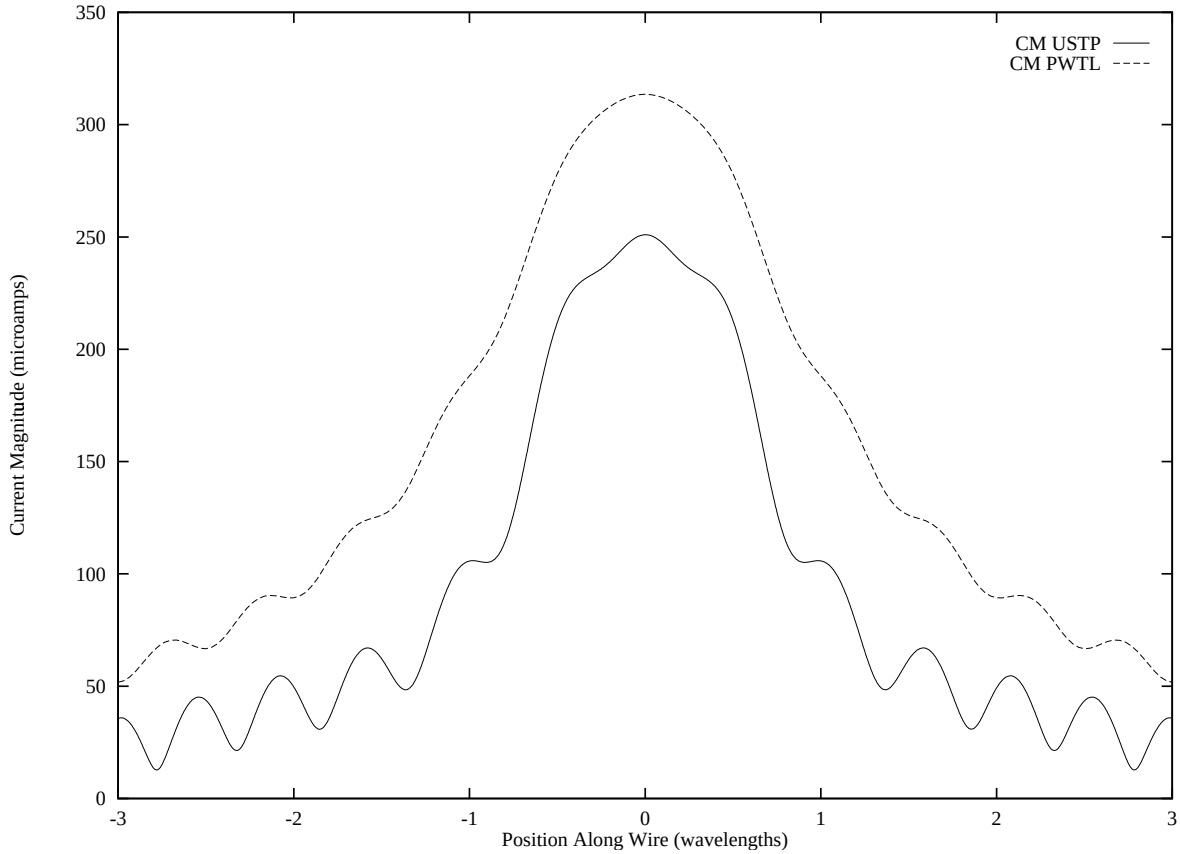

Figure G.35: Common mode current induced on a 6 λ section of USTP by a dipole in configuration 6 at a range of 1 λ (1 GHz). The current is compared with that induced on PWTL in the same configuration.

culties until we had a better understanding of the problems involved. Later simulations used parameters corresponding to real cables. In particular models using CAT-5 UTP parameters in Appendix H were extensively studied. Using these parameters we have to be very careful with the segmentation used in NEC particularly at sensitive termination. To obtain a reliable representation of the structure of the USTP eight to twelve small pieces of wires are needed to model each twist on each of the conductors in the cable giving 16-24 segments per twist and therefore about 350 segments per wavelength at 1 GHz. This limits the detailed model of USTP to about ten wavelengths at 1 GHz with 256 Mb of RAM. The detailed model is therefore only of practical use in modelling small, sensitive, pieces of cable such as terminations. It is also useful in guiding the single wire model of USTP discussed later.

The common and differential mode currents induced on USTP with the above parameters were calculated for a variety of antenna configurations. The differential mode current is always small, typically about 1 mA. The common-mode current for a typical case (dipole at 0.3 m, orientated along the line for maximum coupling) is shown in Figure G.36. The comparison with USP demonstrates the insensitivity of common-mode to the details for the cable structure.

G.9.2 Shielded Pair

Shielded Pair behaves as a single conductor as far as the common-mode pickup on the shield is concerned. To determine the current induced on the internal conductors a transfer function is

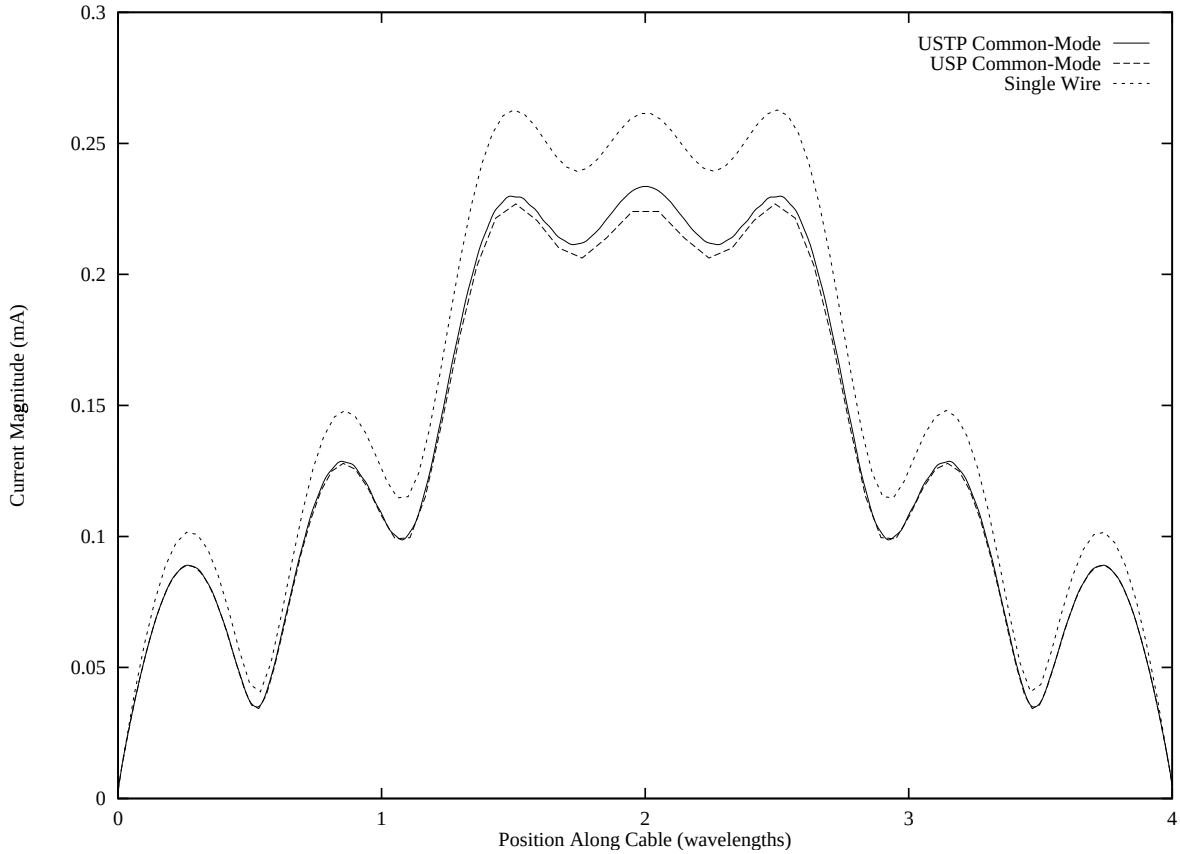

Figure G.36: Common-mode pickup on USTP compared with USP.

used.

The basic problem is depicted in Figure G.37. An EM wave strikes the cable shield inducing a surface current density. This current then produces interference on the internal signal conductors The current on the shield surface can be calculated using the NEC single wire model discussed above. Transfer functions can then be used to calculate equivalent interference sources on the transmission line which are summed to yielded a combined EMI signal in the terminating impedances. The transfer functions are determined by the shield and transmission line parameters and the frequency(s) of the electric field.

G.9.3 Single Wire Models

The excitation and pickup of common-mode currents by multi-wire transmission lines is relatively insensitive to the detailed geometry of the conductors; the cable essentially behaves as a single conductor with some effective diameter. This allows us to consider using a single wire to determine the common-mode current induced on various types of transmission line and then using termination models at allow for mode conversion and hence determine the differential-mode current incident on a device. This method is also much more efficient numerically, especially for twisted pair where we can only model a short length of cable with the detailed bifilar helix model.

Figure G.38 shows the common-mode pickup on a single wire compared to that induced on parallel wire and twisted pair transmission lines in the same configuration. As can be seen, the single wire is quite adequate for predicting common-mode currents. If necessary it is also

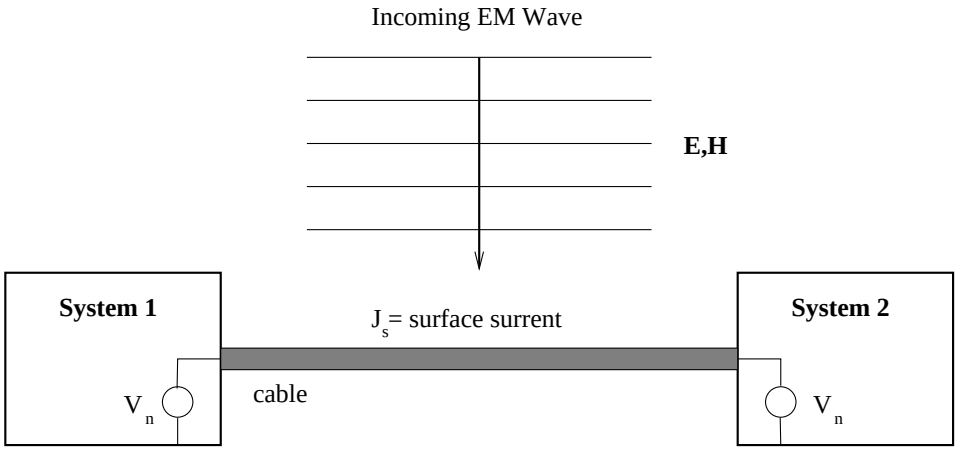

Figure G.37: EM wave striking a screened interconnect cable.

possible to tune the amplitude of the current on the single wire to that obtained in the detailed model, or indeed to experimental predictions, by including a numerical factor since the model is linear.

G.10 Summary

When considering the threat posed to wired networks by multiple source distributed over the bandwidth of a particular system we must consider the level of cable coupling and the propagation of the interference signal picked up to the ends of the cable. In order for wide band EMI from ensembles of mobile radio sources to be detected in cable loads a number of things are required:

1. A number of sources operating on widely spaced frequency channels in close enough proximity to the cable to couple significant energy into differential or common mode currents. Each source will have a zone of interaction with the cable in which the level of coupling is significant - outside the zone of interaction the coupling can be neglected.

2. Sources generating differential mode currents must be close to the ends of the cable in order for them to be effective due to the high differential mode attenuation of most cable at high frequencies.

3. Sources generating common mode currents can have an effect at much larger distances from the cable loads since the common mode attenuation is generally much smaller than that of the differential mode. There must then be some mechanism close to the cable ends which can cause mode conversion from common to differential modes in order for the interference to enter the functional signal paths. Typically this is provided by connectors.

Figure G.39 illustrates this schematically. Six sources (1 to 6) are in the vicinity of a cable running between two pieces of equipment A and B. Equipment A has a high quality balanced

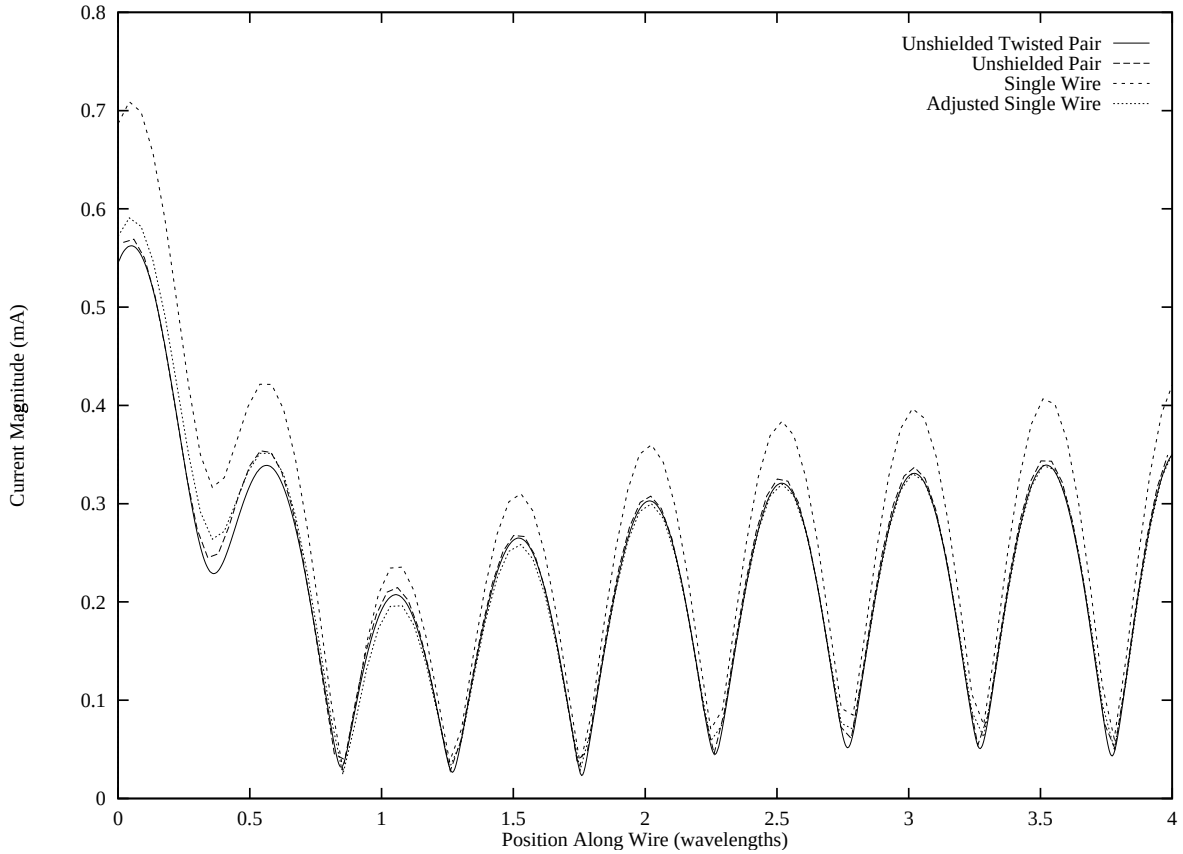

Figure G.38: Common-mode current induced by a dipole source on PWTL, USTP and a single wire in the same configuration. (Dipole orientated along cable at a range of one wavelength situated at the left hand side of the figure).

connection to its internal electronics whereas equipment B has a poor unbalanced connection. Sources 1 and 2 are too far away from the cable to couple any significant energy. Sources 3 to 6 all generate differential and common mode currents within their zones of interaction, however only source 3 is close enough to the equipment for the direct differential mode pickup to reach the equipment electronics. The common mode currents from sources 3 to 6 reach both ends of the cable. Equipment A has the balanced connection so the common mode does not enter the electronics but at equipment B's connection a significant proportion of the common mode current is converted to differential mode and enters the electronics.

To compare the free space propagation loss with that of the cable consider the case if source 6 were 5 m along the cable from B and 1 m away from the cable. The field incident on the cable just before B would be about 13 dB lower than that immediately next to the source. The common mode propagation loss could be significantly lower than this, depending on the details of the environment.

References

[1] C R Paul *Introduction To Electromagnetic Compatibility,* Wiley Series In Microwave And Optical Engineering, John Wiley, 1992.

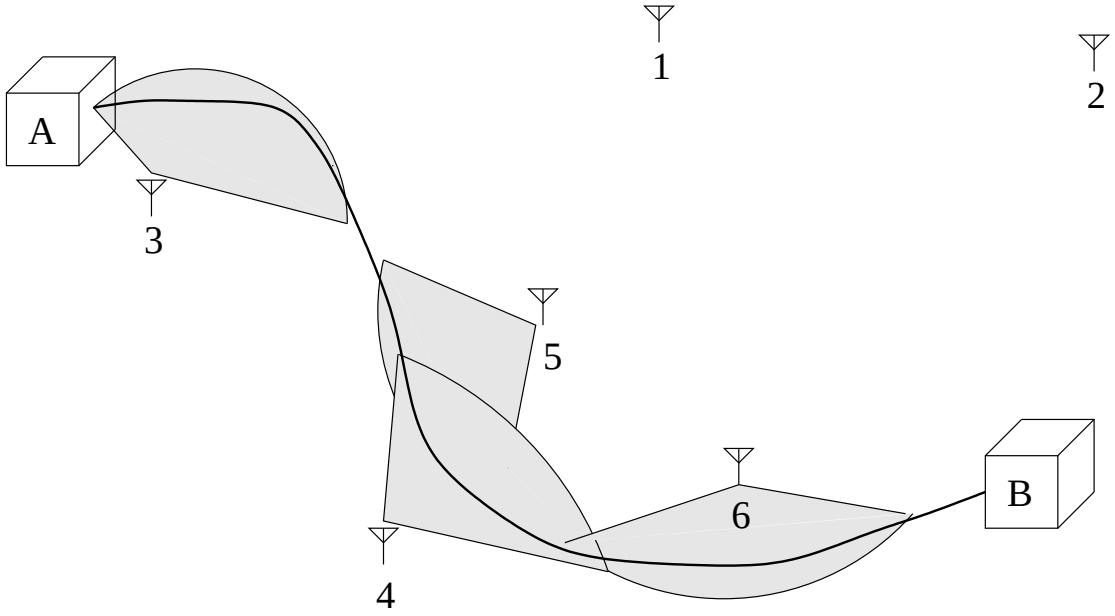

Figure G.39: Schematic of a wired network illustrating pickup from multiple sources.

[2] D M Pozar *Microwave Engineering,* Second Edition, John Wiley, 1998.

[3] M Leininger *Computation Of The Influence Of External Fields On Inhomogeneous Multiconductor Transmission Lines,* Electromag. Compat. Symp., Zurich, 1993, pp. 439-444.

[4] A Smith *Coupling Of External Electromagnetic Fields To Transmission Lines,* Wiley Interscience, New York, 1977.

[5] A K Agrawal, H J Price and S H Gurbaxani, *Transient Response Of Multiconductor Transmission Lines Excited By A Nonuniform Electromagnetic Field,* IEEE Trans. Electromag. Compat., Vol. 22, No. 2, pp.119-129, 1980.

[6] J A Roden, C R Paul, W T Smith and S D Gedney, *Finite-Difference Time-Domain Analysis Of Lossy Transmission Lines,* IEEE Trans. Electromag. Compat., Vol. 38, No. 1, pp.15-24, 1996.

[7] C R Paul *Incorporation Of Terminal Constraints In The FDTD Analysis Of Transmission Lines,* IEEE Trans. Electromag. Compat., Vol. 36, No. 2, pp.85-91, 1994.

[8] C R Paul *A SPICE Model For Multiconductor Transmission Lines Excited By An Incident Electromagnetic Field,* IEEE Trans. Electromag. Compat., Vol. 36, No. 4, pp.342-354, 1994.

[9] K Li, A Tassoudi, R T Shin and J A Kong, *Simulation Of Electromagnetic Radiation Ans Scattering Using A Finite Difference Time Domain Technique,* Comput. Appl. in Eng. Education, Vol. 1, No. 1, pp.42-62, 1992.

[10] G F Pedersen *Amplitude Modulated RF Fields Stemming From A GSM/DCS-1800 Phone,* Wireless Networks, Vol. 3, No. 6, Nov. 1997, pp. 489-598.

[11] F M Tesche *Principles And Applications Of EM Field Coupling To Transmission Lines,* Electromag. Compat. Symp., Supplement, Zurich, 1995, pp. 21-31.

[12] Y Kami and R Sato *Circuit-Concept Approach To Externally Excited Transmission Lines,* IEEE Trans. Electromag. Compat., Vol. 27, No. 4, pp.177-183, 1985.

[13] G J Burke and A J Poggio *Numerical Electromagnetics Code (NEC) - Method Of Moments.* Technical Report UCID-18834, Lawrence Livermore National Laboratories, 1981.